Static Force Production Analysis in a 3D Musculoskeletal Model of the Cat Hindlimb

A Thesis
Presented to
The Academic Faculty

by

Lale Korkmaz

In Partial Fulfillment
of the Requirements for the Degree
Master of Science in the
Woodruff School of Mechanical Engineering

Georgia Institute of Technology
March 2004

Static Force Production Analysis in a 3D Musculoskeletal Model of the Cat Hindlimb

Approved by:

Dr. Lena Ting, Advisor

Dr. Imme Ebert-Uphoff, Co-advisor

Dr. Marc E. Levenston

Dr. Thomas J. Burkholder

April 07, 2004

To my dad,
Fevzi Korkmaz

ACKNOWLEDGEMENTS

I want to thank my family, my mother Sukran Korkmaz, and my brother Cevat Korkmaz for their incredible fidelity during my studies in the USA. With her joyful voice through the telephone lines, my mother gave me the strength and encouragement I needed. Cevat gave me calmness and made me smile when times were hard with his jokes through messaging and e-mails.

I want to thank Tyler Hunt, his mother Suzzette Hunt, and his father Jim Hunt. Tyler was understanding and helpful in every aspect during my stressful working days. He helped me set realistic goals and seeded the desire to accomplish those goals. Tyler's family, through their comfort and support, made me feel at home.

I would also like to thank my advisor Dr. Lena Ting, co-advisor Dr. Imme Ebert-Uphoff, and Dr. Thomas Burkholder. Without my advisor's motivation and illuminating power, I would not accomplish this work. Most important of all, she taught me how to learn and explain what I know. Also, my co-advisor and her students were there whenever I had a question in mind. Dr. Thomas Burkholder shared all of his experimental-modeling data and knowledge with me. Whenever I knocked on his door, he had time to help me.

I want to thank my lab-mates Gelsy Torres-Oviedo, Lucas McKay, Kartik Sundar, and Jun Li for their aid in this thesis and their friendship in and outside of the lab. I gained many possessions at the same time: a degree, knowledge, and friendship.

TABLE OF CONTENTS

LIST OF TABLES

LIST OF FIGURES

SUMMARY

To understand control strategies employed by the central nervous system (CNS) control movement or force generation in a limb, a seven degree of freedom cat hindlimb was modeled. In this study, the biomechanical constraints affecting force generation for balance and postural control were investigated. Due to the redundancies at the muscular and joint levels in the musculoskeletal system, even the muscle coordination pattern to statically produce a certain amount of force/torque at the ground is not straightforward.

A 3D musculoskeletal model of the cat hindlimb was created from cat cadaver measurements using Software for Interactive Musculoskeletal Systems (SIMM, Musculographics, Inc.). Six kinematic degrees of freedom and 31 individual hindlimb muscles were modeled. The moment arms of the muscles were extracted from the software model to be used in a linear transformation between muscle activation, and end effector force and moment. The Jacobian matrix that establishes the relationship between joint torques and end effector force was calculated. Maximal muscle forces were estimated from the literature. A feasible set of forces that can be generated at the toe was constructed using combination of maximally activated muscle excitations. Because the endpoint torque is typically small in a cat, an optimization algorithm was also performed to maximize the force generation at the end effector while constraining the magnitude of the endpoint torque. The results are compared with the measured force magnitude and direction data from an acute cat hindlimb preparation for different postures. This static

model is applicable for understanding muscle coordination during postural responses to small balance perturbations.

I. INTRODUCTION

1.1 Background and Significance

Ordinary movements such as walking, running, moving our head, arms and legs, jumping, etc. are performed by the precise coordination of our musculoskeletal system and our central nervous system. Balance in humans is necessary to perform these motions. Balance is accomplished by the control of action forces generated by our limbs and body, and the reaction forces of the contact surfaces, e.g. the ground. This study addresses the questions of how muscles are coordinated by the nervous system to produce forces for balance control.

This work is inspired by neuromechanical strategies found in cat balance experiments (Macpherson 1988a, 1988b). From experiments in postural control it was not clear whether the strategy taken by cats to maintain balance was governed by biomechanical or neurological constraints. A cat hindlimb in three-dimensions was modeled to understand the biomechanical constraints that influence balance control. The cat was chosen because of the large literature in muscle coordination and neural control of movement (Horak and Macpherson, 1996; Rossignol, 1996).

Previous experimental work has contributed to our knowledge of biomechanics, sensory feedback, and spinal cord circuitry during movement (Murinas 2003; Burkholder and Nichols, 2000; Macpherson, 1988a,b). These experimental works were used to generate and validate our model. Joint axes, origins, and muscle connection points used in our

model were acquired from morphological data in postmortem cats (Burkholder and Nichols, 2000). For validation purposes, end point forces calculated in our model were compared to recorded end point forces obtained from single muscle stimulations in acute cat experiments (Murinas 2003).

As an example of experimental work that can benefit from our model, we mention the automatic postural responses in the cat long studied by Dr. Jane Macpherson. In Macpherson's postural experiments on behaving cats "the force constraint strategy" was found, which is a stereotyped force response to balance perturbation (Macpherson, 1988a). Cats freely standing on a platform were perturbed by horizontal translations of the platform in multiple directions. Results showed that stabilizing forces generated by the cats were applied along only two lines of action regardless of the perturbation direction. The orientation of those lines of action was found to be towards or away from the center of mass of the cat, along a roughly diagonal axis. These results implied that the central nervous system may simplify balance control by generating forces in lines of action towards or away from the center of mass. The force magnitude at each paw is modulated so that the combination of the force vectors applied by all four paws is in equal amount and opposite direction to the perturbation. Therefore, the force constraint strategy successfully restores animal's center of mass.

The overall study does not reveal the uncertainty of whether the mechanical constraints or the neural constraints enforce the "force constraint strategy". Our aim is to determine to what extent the source of the force constraint strategy is the biomechanics of the limb,

or some neural control mechanism. We studied how linkage mechanics and posture affect end point forces generated by the limb. For example, if the mechanics of the limb allows forces to only be applied in a specific direction, the limb will be constrained to generate a force in only this direction independent of the neural inputs.

However, further experiments by Dr. Macpherson suggest that there may also be kinematic constraints on force production that change with limb posture. When cats stand with their feet closer or further away from each other in the sagittal directions, the force constraint strategy changes. For longer stance distances compared to preferred, the forces are more strictly aligned along the diagonal axes for all perturbation direction. In contrast, for shorter distances, a relaxation of the force constraint occurs whereby the forces are more distributed over all directions.

Taking Dr. Macpherson's point further, Dr. Richard Nichols' Lab investigated the endpoint forces of individual muscles. The toes of decerebrate cats were connected to a force/torque sensor and hips were fixed. Individual muscles were stimulated differentially in vivo (intramuscularly) in three animals and detailed horizontal force measurements were taken (Murinas, 2003). Intramuscular recordings of seven muscles on the right leg in quiet stance were compared with recordings during crossed extension reflex. Crossed extension reflex is the extension of a leg when the contra-lateral leg is flexed due to a cutaneous stimulus, causing a flexor-withdrawal reflex.

The results of the experiments showed that all the muscles activated produced 3-D forces and not only forces in the sagittal plane. The direction of the forces generated at the toe for a muscle was consistent across subjects, experiments and different limb configurations. The force amounts increased as the muscle stimulation rates increased. The experimental data supplied by Dr. Nichol's Lab was helpful in ensuring the overall processes used in our model. In the experimental data, the joints were free to move, whereas in our model the joints were presumed to be stiff. However, the directional force information employing differentially stimulated muscles provides a source of validation for our analysis.

1.2 Neural Control Mechanism

The motor control mechanism of the CNS and biomechanics are related to each other. The central nervous system gives muscles or, in biomechanics language, "actuators" a command, or "control signal", through efferent pathways. The aim is to accomplish task-level goals like positioning the hand next to a glass of water-- "kinematics"; or applying a certain amount of force on the glass--"kinetics". The sensory feedback system sends information gathered about the kinetics and kinematics of the arm back to the central nervous system.

The feedback system and the intrinsic mechanical properties of the musculoskeletal system work together to stabilize the body. In this context, the feedback system is composed of the proprioceptive feedback system, cutaneous feedback system, and visual and vestibular systems. The proprioceptive feedback system is formed by Ia, Ib and II

afferents located in the muscles (muscle spindles and Golgi tendon organ). These sensors provide information about the muscle length, velocity and force.

In the musculoskeletal systems, there are many muscles and joints that provide different force-torque generation capabilities. The mechanical characterstics of the musculoskeletal system also change for different postures. These redundancies allow the lower level control mechanism the flexibility to choose among different patterns to accomplish a task-level goal.

Two types of redundancies are inherent in our musculoskeletal system: muscular level and joint level. Firstly, two muscles are enough to apply torque around a mechanical joint in both directions. Muscles can only produce forces in tension. As the muscle contract, they pull the bones. In the musculoskeletal system, the number of muscles crossing each joint is much greater than two. Therefore, the same joint torque can be applied with different muscle configurations. Also, one muscle can cross more than one joint. Secondly, there are more joints than the degrees of freedom of the end point of the limb. Specifically, the end point of the limb has six degrees of freedom in a three dimensional space and three degrees of freedom in a two dimensional space. When muscles are activated, they apply torques around the joints. Thereby, the same postural response can be performed by several different combinations of the joint torques. Then, the relationship between the end effector force and the joint torques is one to many.

Despite the biomechanical redundancies the CNS appears to respond to postural perturbations with a rather simple force constraint strategy. Therefore, there must be a coupling between the biomechanics and neural control. We are interested in the question of whether the biomechanical constraints of the leg, such as joint locations and orientations, and muscle force-generating properties determine the actions of the leg during automatic postural responses in the force constraint strategy. Also, we are interested in whether there are higher level neural mechanisms which control the posture, movement and kinetic characteristics of the musculoskeletal system, such as a central pattern generator as speculated by some researchers (Marder and Calabrese, 1996). We developed a model and an analysis technique to address these questions.

1.3 Hindlimb Model in SIMM

SIMM (Software for Interactive Musculoskeletal Systems, Musculographics, Inc.) is an appropriate graphical tool for extracting the necessary parameters to calculate the joint torques and doing biomechanical analysis of the cat hindlimb. SIMM enables the anatomical construction and kinematic and kinetic analysis of musculoskeletal systems. Musculotendon lengths, moment arm, moment and force values of the muscles can be obtained for different joint angles. Inverse and forward dynamic simulations can also be done. One can specify a muscle coordination pattern for postural control and get back the muscle forces and moments for any position of the body. It is user friendly, has great graphics, its computations are easy. It allows three-dimensional visualization of the biomechanical systems. Biomechanical researchers, neuroscientists, medical students, kinesiologists, human factors engineers, biologists, computer scientists, and animators

utilize SIMM. A wide variety of realistic musculoskeletal structures can be developed interactively (Gonzalez et al., 1997; Schutte et al., 1997; Free and Delp, 1996).

SIMM uses the Hill model (Zajac, 1989) for acquiring force production and length characteristics of the muscles. Generally, an average muscle is composed of a hundred muscle fibers, each innervated by a single motor neuron close to its middle point. Motor neuron inputs, velocity and length properties of the muscle shapes its output force. The Hill muscle model has a contractile element and parallel and serial spring elements in each muscle as seen in the Figure 1. The primary muscle tissue is represented by the contractile element whereas the parallel elastic element represents the connective tissue infrastructure, such as the musculotendon sheath, the muscle fiber membranes, and the overall fluid environment within which muscle tissue lives.

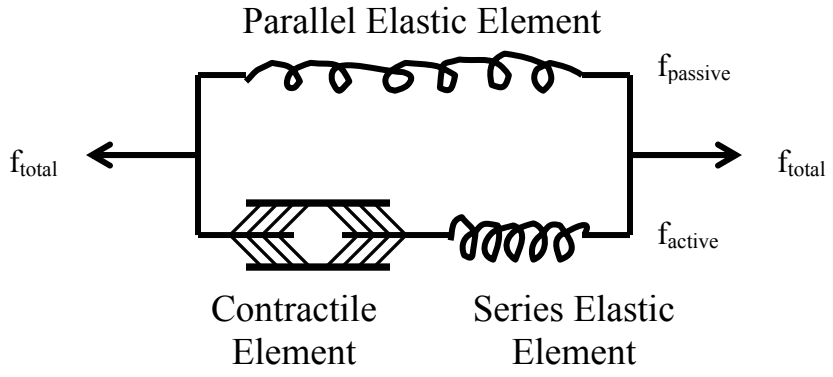

Figure 1: Elements of the Hill Muscle Model.

The relationship between the force-length (Figure 2) and force-velocity (Figure 3) characteristics of the muscle is nonlinear. Contrary to a spring/linear elastic element,

their relationship cannot be represented by a straight line and a single parameter. The muscle contractile element applies its maximum force at an intermediate length. If the length is increased or decreased more than that intermediate length, then the force applied decreases. The effect of the parallel passive element is an additional force application as the length of the muscle increases from its resting (Lo) length exponentially. Force generated by the muscle increases during eccentric contraction (a muscle lengthens while activated) up to a plateau as the velocity is increased and decreases during the concentric contraction (a muscle shortens while activated) as the velocity increased.

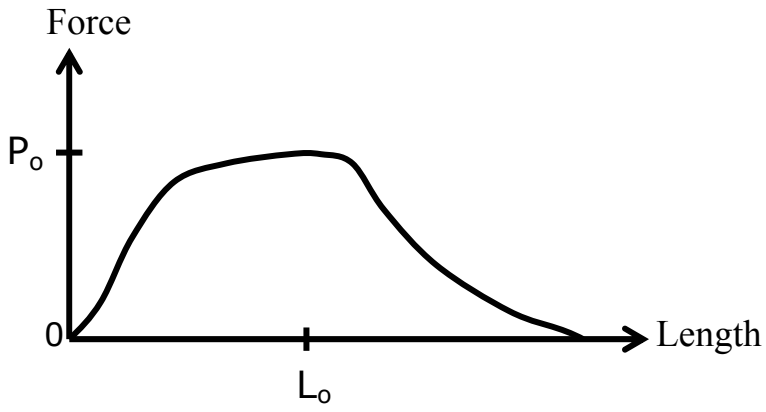

Figure 2: Force-length characteristics of the Hill Model contractile element.

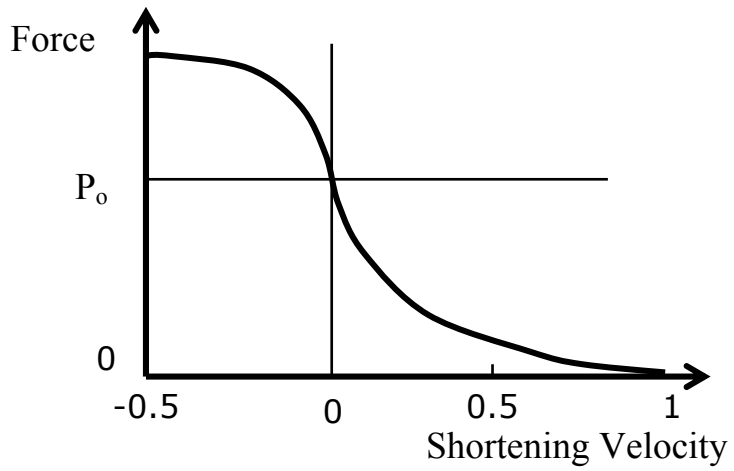

Figure 3: Force-velocity characteristics of the Hill Model contractile element.

The data to create the input files for the SIMM cat hindlimb model was supplied by Dr. Burkholder (Burkholder and Nichols, 2003). Three dimensional architecture data was available for some muscles in the literature (Sacks and Roy, 1982; Loeb and Richmond, 1994). Dr. Burkholder conducted experiments to gather the unavailable data for other muscles, i.e. gluteus medius, gluteus maximus, and psoas. The three dimensional muscle connection points and joint kinematics were not known prior to Burkholder. The cat hindlimb models were in two dimensions and had to incorporate two dimensional muscle and joint parameters (He et al., 1991). He made experimental measurements on three dimensional muscle and joint parameters such as muscle connection points to the bones, and joint rotation positions and axes. The Burkholder model was coded into "CompleteCat.def" file as an input to the software DADS (Dynamic Analysis and Design Software, LMSCADSI, Coralville, IA). All of the parameters necessary for the default posture of the SIMM model were characterized by the Burkholder model which was validated by the experiments of Dr. Nichols and studies in the literature (Young et al.

1993), and was used to show the effects of proprioceptive length feedback (Burkholder and Nichols 2000). Thus, the overall joint and muscle kinematics and force results were compared in between the two models for verification purposes. Hip joint motion was considered in the force analysis despite the thigh was fixed in the input model. We checked if the generated forces matched the experimental ones.

1.4 Mechanical Analysis

The Jacobian matrix in a kinematic analysis maps joint velocities to end point velocities. A mathematical tool, the Jacobian matrix is used in the areas of robotics and biomechanics to do kinematic, static, and dynamic analysis. Forward kinematics and inverse kinematics are two types of positional and velocity analyses of a linkage system that can be performed with the Jacobian representation. In forward kinematics, the joint angles and link structure are known, and desired positions (e.g. end point) are calculated. On the other hand, in inverse kinematics, it is the joint angles that are calculated from the segmental positions.

The Jacobian matrix links the knee and ankle joint torque to an action force and moment at the toe. In static analysis, the Jacobian matrix is a tool to handle a mapping between joint torques and end point force-moment. The muscles generate forces, and apply torques about the joints based on the positions of the muscle-bone connections. Joint torques are transmitted to an end point of the musculoskeletal structure. The Jacobian matrix, which depends on the limb posture and muscle forces, is an approach to handle this transmission. For example, the gastrocnemius muscle orginates just above the knee

and inserts in the calcaneous of the foot. Thus, when gastrocnemius is activated, it applies a torque around the knee and ankle joints. This torque is transmitted to the end point and the lower part of the leg.

In our study, static analysis was utilized for investigating very small movements. The postural control experiments performed by Macpherson (1988a) involve small perturbations to standing balance. Since the response to perturbations introduces differential movement of the segments and therefore joint angles, a static model is practical in our research for testing further hypotheses.

The Jacobian method is used widely in the area of robotics in a variety of robots with extensive capabilities. Manipulator structures such as three-link planar arm, Puma 560 industrial robot, Anthropomorphic arm, Stanford Manipulator (Sciavicco and Siciliano, 2000), modular robots (Tarchanidis 1995), and modular reconfigurable robots (Chen, et al., 1999) employ the Jacobian matrix. Modular robots help the user construct the robot in different configurations for different applications.

The Jacobian method is utilized considerably in the biomechanics literature, too. Valero-Cuevas' studied the muscle coordination patterns of the human index finger producing maximum force at the distal phalanx (Valero-Cuevas, et al. 2003). The four degree of freedom static model is three dimensional and has seven muscles. Optimization to the end-effector force application of the index finger was performed by computational geometric principles. Experiments were performed on human subjects to whom it was

instructed to apply maximum static forces at the distal phalanx of their index fingers. The muscle excitations and end effector palmar force were similar among the predicted and measured results. The model over-estimated the distal and lateral forces generated by the tip of the index finger. Parameters such as moment arms and some maximum muscle forces turned out to be substantial in the predictions.

Another research project similar to the human index finger study was done on the thumb by Valero-Cuevas (Valero-Cuevas, et al. 1998). Eight muscles in three dimensions were recruited for the static maximum force estimations. Experiments were performed and EMG data was acquired. According to the results of the Monte Carlo simulations, they argue that the kinematic description of the thumb is the crucial factor in reflecting the reality more than the musculoskeletal parameters and the solution method.

Some robot manipulators were also inspired by the biomechanical models. Research on tendon arrangements and muscle force requirements for humanlike force capabilities in a robotic finger (Pollard and Gilbert, 2002) is an example where the Jacobian matrix was utilized. The force generation capabilities of the robotic finger which was driven by tendons were optimized. The results indicate that with a couple of arrangements, the same extent of forces generated by the actual human finger can be generated by the robotic finger.

As another musculoskeletal model involving the Jacobian, the three degree of freedom human leg was modeled (Spagele, et al., 1999). The body was consisted of three links,

nine muscles. The ground reaction forces were measured by force plates. The muscle redundancy problem was optimized by applying a multiphase optimal control technique for vertical jumps in sagittal motion. The forward dynamic optimization was performed for minimal muscle activations and maximum height jumping. There was a close relationship between the estimated muscle activations and the experimental EMG values.

Musculoskeletal structures are redundant and thus statically indeterminate systems governing the assignment of muscle activations, muscle forces, and joint torques which the Jacobian matrix cannot solve. When the number of unknowns equals the number of independent equations, the system is statically determinant and the solution is unique. On the other hand, for statically indeterminate systems, the number of unknowns exceeds the number of equations. There are different ways to solve the statically indeterminate problems such as increasing the number of constraints, or utilizing optimization techniques. In the first approach heuristics are used, in the latter, a cost function is introduced. Both approaches were employed in this study.

Leading to the solution of the redundant problem, optimization is an indispensable tool in biomechanics. Different optimization methods such as gradient-based, parameter optimization algorithm, variational approach (Pandy et al., 1992), modified Polak-Mayne algorithm (Pandy et al., 1990), stochastic optimal feedback control (Todorov and Jordan, 2002), and Fourier-based methods (Nagurka et al., 1990) were used in the literature depending on the static-dynamic or linear-nonlinear nature of the problem (Raikova and Aladjov, 2002; Happee 1994; Bean and Chaffin, 1988).

II. THE SIMM MODEL

2.1 Model Development

The right hindlimb of the feline was modeled by utilizing digitized data from a previous model by Dr. Burkholder (Burkholder and Nichols, 2000). In the Burkholder model, the major bones and muscles were modeled on the basis of measurements taken from five cats. The pelvis and the toe were fixed approximating the natural stance configuration of the leg.

2.1.1 Main Features of the Model

The static three-dimensional musculoskeletal model was created to examine the force generating capabilities of the cat hindlimb. A wide range of muscle and joint parameters were used to construct and validate the biomechanical model. The static model represents the system adequately to a first approximation because perturbations to the hindlimb result in small changes in joint angles. The three dimensional model is advantageous over the previous two dimensional models of the cat hindlimb (He et al., 1991; Prilutsky et al., 1997; Hof, 2001) in reflecting the non-sagittal components of the forces generated by the leg.

The seven degree of freedom model consists of three anatomical joints: hip, knee and ankle; and five mechanical joints: hip, knee extension, knee adduction, ankle extension, and ankle adduction. The hip is a spherical joint (3 d.o.f.), whereas, the other four are pin

joints (each 1 d.o.f.). The hip connects pelvis and femur, knee connects femur and tibia, and ankle connects tibia and foot bones. The toe was also included as an end point to the bones of the model: pelvis, femur, tibia, foot. Each d.o.f. is associated with a rotation axis. In a human who is standing up, biomechanical rotation axes can be defined as follows: flexion-extension, adduction-abduction, and inversion-eversion, collinear with medial-lateral, anterior-posterior, and vertical directions, respectively. Flexion-extension, adduction-abduction and internal-external rotation of the hip joint are performed by the femoral head (a spherical protrusion of femur close to pelvis). They are assumed to intersect at the conceptual center of the femoral head. The flexion-extension and abduction-adduction axes of the knee or ankle joint do not intersect.

As a suitable tool for musculoskeletal modeling, SIMM was employed to calculate necessary parameters such as moment arms and position vectors. SIMM can also be used for further dynamic analysis. For the SIMM model, beside the bone files, two types of files were needed as inputs to the model: the joint file (Section 2.2) and the muscle file (Section 2.3). The joint file retains the connection of bones; the muscle file retains the muscle connection points and their physiological properties.

2.1.2 Data Used: DADS Model

The data for generating the model was supplied by Dr. Thomas Burkholder's three dimensional musculoskeletal model of the feline hindlimb based on digitized musculoskeletal anatomy (Burkholder and Nichols 2003). Five cats were dissected to derive the model. The joint rotation axes were defined using mechanical techniques for

locating non-orthogonal joint rotation axes (Hollister, 1992, 1993). There are seven rotational degrees of freedom in the model. Three rotations were modeled at the hip joint, two at the knee joint and two at the ankle joint. 32 muscles with their connection points to the bones were described in the model.

The Burkholder model was implemented in DADS software which is not well-suited for musculoskeletal modeling. DADS is a mechanical simulation software that performs kinematic, static, forward dynamic, and inverse dynamic analyses for mechanical models. However, because DADS is a general mechanical modeling package, it is not well-suited for calculating variables of interest to musculoskeletal modelers, such as musculotendon length, moment arm, moment and force values of the muscles. While some of these variables can be calculated through some tricks and additional tools, others can not be calculated at all. Further integrating a muscle model for dynamic simulations requires that the DADS model be linked to a MATLAB (the MathWorks Inc., Natick, MA, USA) muscle model.

On the other hand, SIMM is specifically for musculoskeletal systems and allows the user to visualize all of the muscle paths as well as output many biomechanically relevant variables. Dynamic simulations of the musculoskeletal models created in SIMM can be performed by integration with Dynamics Pipeline (Musculographics, Inc.). Dynamics Pipeline calculates the motion of the body with respect to known muscle activation patterns for forward dynamics. For inverse dynamics, positions, velocities and accelerations of the generalized coordinates (e.g. joint angles) are specified and the

software calculates the joint torques necessary to produce the motion. As mentioned, in SIMM activation patterns can be assigned to muscles and even the muscle models can be customized.

To construct the model, each limb segment has its own reference frame and rotation axis defined in that reference frame. There are four physiological bones in the DADS model. DADS uses different coordinate systems (CS) for each segment/bone. Bony landmarks are used for defining the reference frames for the 'Muscle Coordinate System' of each segment, i.e. Pelvis Muscle CS, Thigh Muscle CS, Shank (tibia and fibula complex) Muscle CS, Foot Muscle CS. First, an origin is determined for the Muscle CS of a bone. Two bony landmarks are defined. The first one from the origin along the longitude defines the x axis. Another bony landmark from the origin forms the second vector and is used to define the x-y plane. The cross product of the x axis of the bone and the second vector defines the z-axis. Similarly, y-axis is calculated using the cross product of x and z vectors. The sign convention used is such that in the normal posture of the feline, x is along the longitudinal, or vertical direction, while the y and z axes are directed towards the medial direction and the anterior direction, respectively. A Muscle CS involves muscle attachment points and is defined in a coordinate system called CSYS. In addition to the Muscle CS, DADS uses CSYS and Bone CSs for each bone/segment. The supplementary CSYS coordinate system was created for each bone to define joint axes.

The DADS model input file was converted to SIMM model input files by a transformation process described in the next section. A "CompleteCat.def" file containing all the CSYS and Muscle CS information was created by Dr. Burkholder as an input to DADS simulation software. The joint and muscle files, which are the necessary input files for SIMM were coded using the "CompleteCat.def."

2.2 Conversion from DADS to SIMM Model

In the default limb posture, SIMM has a convention for the orientation of all the segments of the body. The convention in SIMM is to orient the y axis toward negative gravity, and the x axis and z axis cranially and laterally, respectively. This coordinate system convention will be referred as General Coordinate System (GCS). Each segment's local CS has a different origin, but the segment axes are aligned with the GCS in the default limb posture, rather than with anatomical landmarks.

In DADS, the bones, the joint axes and the muscle connection points to the bones are defined in different coordinate systems. Conversions between consecutive reference frames, which are the opposite direction of the arrows in Figure 4, are also defined. The aim is to define all the points of a segment (bone origins, joint axes and muscle connection points) in its local SIMM coordinate system. Local coordinate systems have their axes aligned with GCS in default posture. The hierarchy among all the coordinate systems in DADS and SIMM is shown in Figure 5.

2.2.1 Bones and Transformations

The vector information in the reference frames of the DADS model was transformed to the Global Coordinate System of the SIMM model utilizing rotation matrices and translations. There are many ways to perform the relative rotations between the coordinate systems: the standard x-y-z Cartesian angles, Euler angles, the Euler parameters and so on. There is not a common method characterized among biomechanics researchers. In the DADS model Euler parameters were used.

DADS uses a hierarchical structure. The bones (the coordinate systems) have "parents and children" arranged from proximal to distal. For example, in Figure 4, if we take the segment tibia, its reference frames are Shank Muscle CS, Shank CSYS; its parent is KFSYS and child is AFSYS. Shank Bone CS is not shown in the hierarchy figure because it does not affect the construction of the model. Pelvis and femur were characterized in a coordinate system called "World."

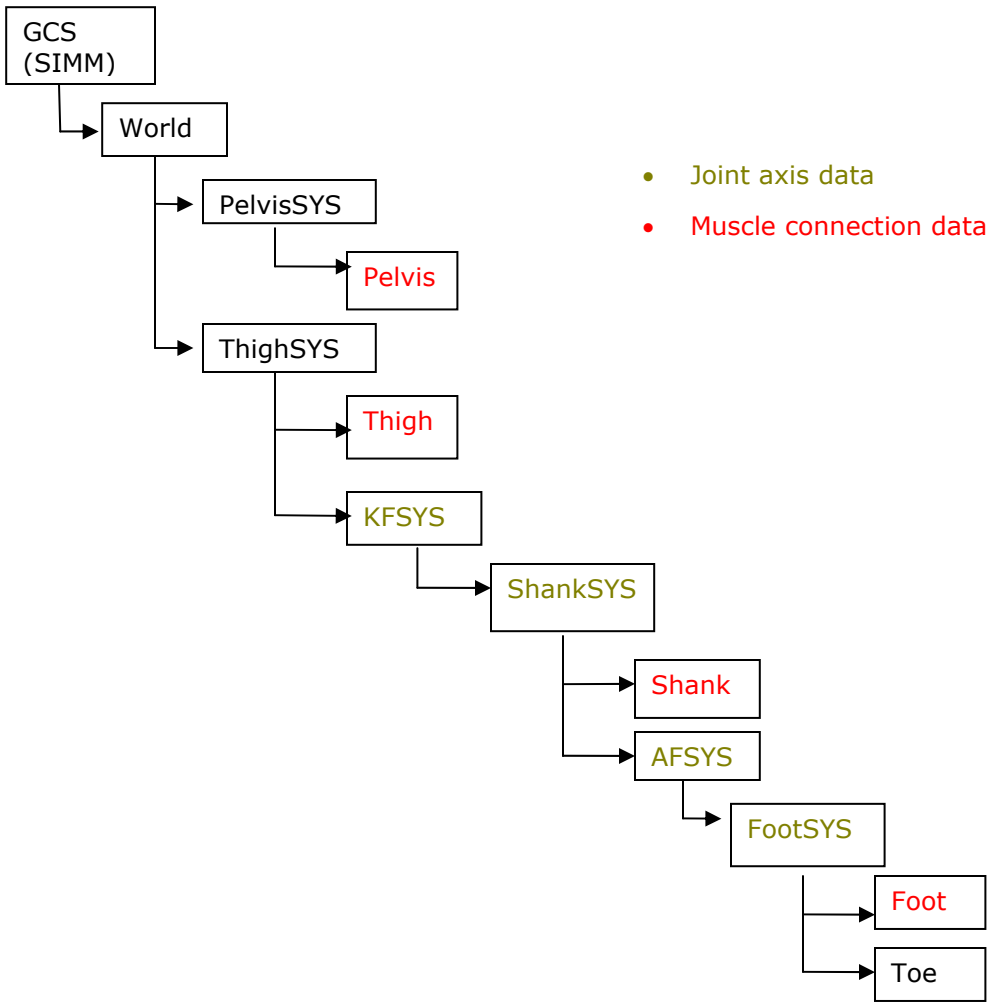

Figure 4: Hierarchy of the coordinate systems of the data used ('CompleteCat.def'-DADS file).

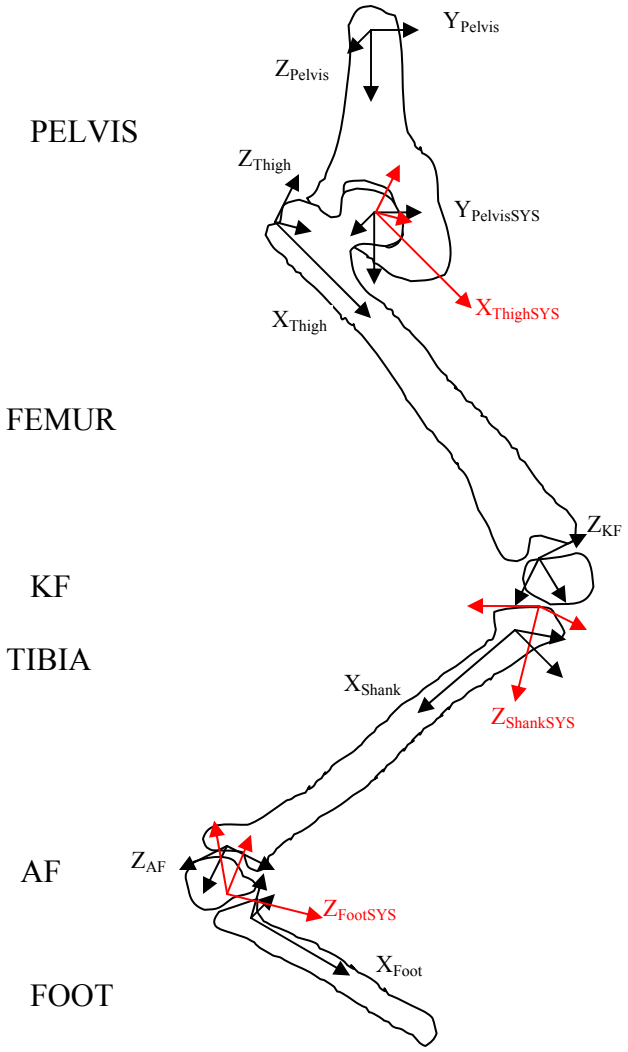

Figure 5: A rough sketch of all CSs of 'CompleteCat.def."

Data points in the coordinate systems were carried through the GCS by rotation matrices. Euler angles were taken from the DADS input file and rotation matrices were calculated by the Euler parameters to find the coordinates in the SIMM GCS and LCS's.

In SIMM the bones are pelvis, femur, tibia, foot and toe, sequentially. There are two intermediate pseudo bones KF and AF, which contribute the two degrees of freedom motions of knee and ankle joints. The knee flexion-extension axis and knee adduction-abduction axis, as measured by Burkholder and Nichols (2000) do not intersect. Therefore, a phantom segment KF (knee flexion) that has the same origin as tibia was created between femur and tibia to include knee adduction-abduction axis in the DADS model. Similarly, AF (ankle flexion) was created for the ankle adduction-abduction axis. The same idea was utilized in the SIMM model. Therefore, the sequence became pelvis, femur, KF, tibia, AF, foot and toe. All the bone files used in the model were laser-scanned by Dr. Burkholder and written into the AutoCAD files These files were converted to suitable polygons that define the bone surfaces as ".simm" files and transformed by inspection to their mechanical origin (Section 2.2.2) and orientation to visualize the default posture. This procedure is performed by inspection and does not show the exact positions and orientations of the bones because in SIMM bones are shown only for visualization purposes.

2.2.2 Joints

The positioning and axes of rotation of all the mechanical joints were determined and written to the SIMM joint file. A bone is connected to the next one via two kinds of

information. The first one is the positioning of the origin of the next bone, and the second one is the orientation of the rotation axis between the two bones. The bone closer to the head is called the proximal bone (segment coordinate system), and the bone close to the ground is called the distal bone. SIMM requires the joint rotation axis between the proximal and the distal bones to pass through the origin of the distal bone. Since the z axis of the CSYS coordinate system in DADS determines the joint axis, the origin of CSYS of each distal bone was selected as the origin of the segment in SIMM. The origins of every distal segment and every joint axis were defined in a SIMM local coordinate system (LCS) of the proximal bone using rotation matrices. Local coordinate systems have axes parallel to GCS in the default posture, but the origins are translated to the joint rotation axes. As the joint angle change, the LCS move with the bone (i.e. the LCS is fixed in the bone). The calculations for the origins of the segments and the joint axes were carried through a MATLAB file. An example is shown below in Section 2.2.3.

2.2.3 Knee Flexion Example

It is demonstrated how to find the distal segment origin and joint axis in GCS in knee flexion. Knee flexion is a pin joint connecting the bones femur and KF. The origin and the joint axis of knee flexion were calculated in femur LCS. 'CompleteCat.def' provides the data, i.e. the origin of KF and the joint axis of the knee flexion in ThighSYS CS. We found the origin of KF and the joint axis (green and dashed vectors in Figure 6) in femur LCS (black and dashed vectors in Figure 6).

According to the hierarchy of Figure 4, the data of ThighSYS CS were transformed to the World CS. The origin of KF in femur was found by rotating the origin vector in ThighSYS CS to femur's GCS.

$$R_{femur} = R_{femurLCS}^{World} \cdot R_{World}^{ThighSYS}$$

$$O_{KF} = R_{femur} \cdot O_{KFOrigin}^{ThighSYS}$$

where, R is the rotation matrix transforming the elementary basis vectors of the coordinate system in the superscript to the coordinate system in the subscript, and O's are the vectors from the origin of the coordinate system in the superscript to the origin of the coordinate system in the subscript.

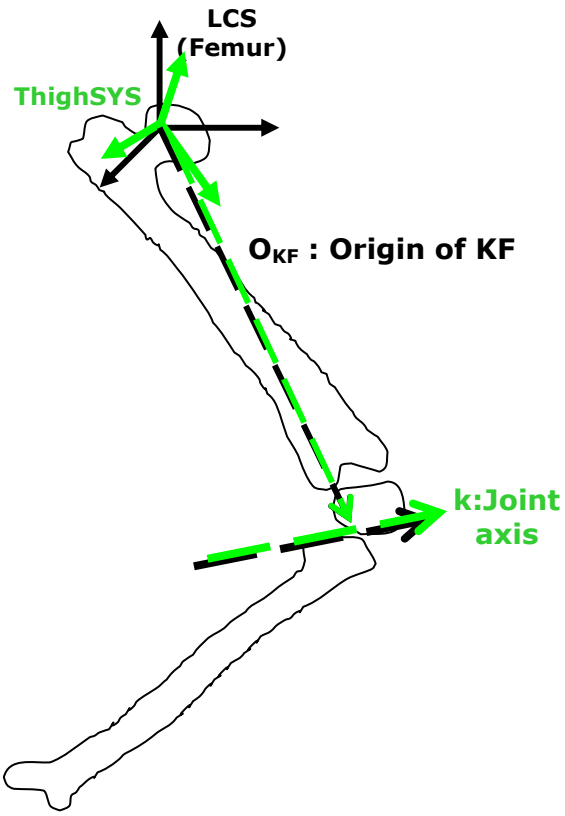

Figure 6: A sketch showing the phantom KF bone origin and the knee flexion joint axis.

The joint axes are the z axes of the green reference frames in Figure 6. In this example, the knee flexion joint axis is the z axis of KF. As a phantom segment, KF is special since its CSYS and Muscle CS are the same and named as KF. The rotation is computed and the vector pointing knee flexion axis is rotated to femur's LCS as follows:

$$R_{KF} = R_{femurLCS}^{World} \cdot R_{World}^{ThighSYS} \cdot R_{ThighSYS}^{KF}$$

$$k_{KF} = R_{KF} \cdot \begin{bmatrix} 0 \\ 0 \\ 1 \end{bmatrix}$$

where rotation axis is denoted by k.

2.2.4 Posture of the Hindlimb

By SIMM convention, the joint angles are defined to be zero for the measured, or default posture of the leg. The posture can be expressed in a more convenient way by calculating the angles between the bones. Thus, the hip, knee and ankle angles correspond to the angles between the bones pelvis-femur, femur-tibia, and tibia-foot.

It is possible to compute the anatomical joint angles from the SIMM model with a linear algebraic procedure. The x axes of the Pelvis, Thigh, Shank and Foot CSs in the 'CompleteCat.def' data are along the longitudinal axis of the bones. Figure 7 represents the orientation of the x-axes. We can transform these axes using rotation matrices to express all the vectors in the same CS. Then the problem is simplified to finding the angles between two vectors using the dot product.

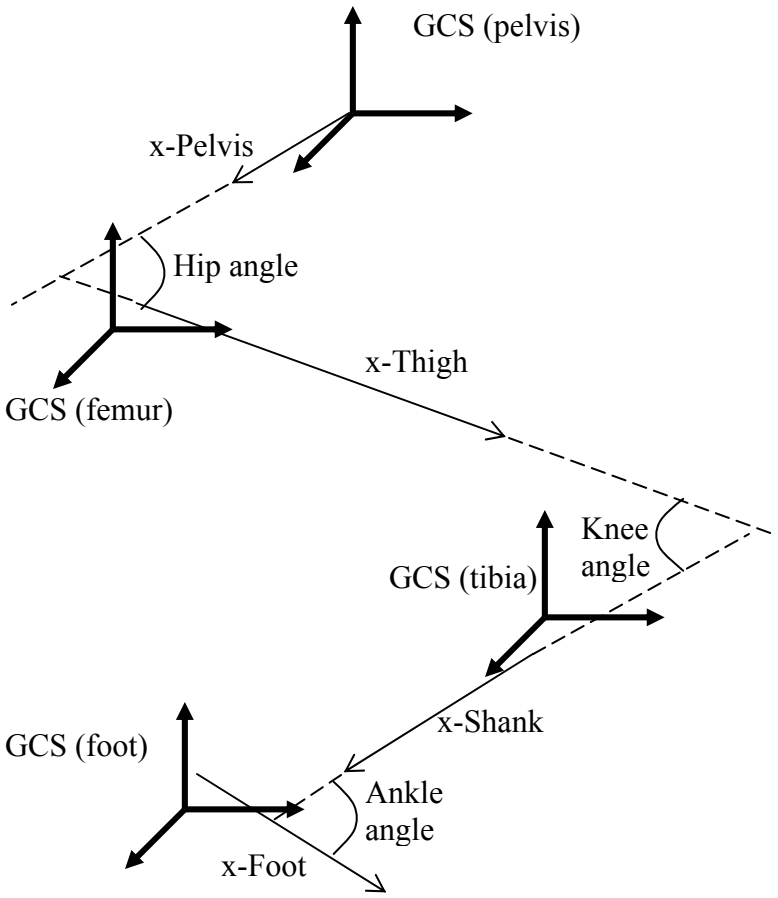

Figure 7: Sketch showing the longitudinal axis (x-axis) of the bones and the knee angle between the hindlimb bones.

The dot product of two vectors is equal to the multiplication of their lengths with the cosine of the angle between them:

$$\vec{a} \bullet \vec{b} = |a| \cdot |b| \cdot \cos(\theta)$$

Since the x-axis vectors are unit length, the dot product gives the cosine of the angle. For example, the knee angle is calculated by the dot product of x-axis of Thigh CS and x-axis of Shank CS.

$$\vec{x}_{Thigh} \bullet \vec{x}_{Shank} = \cos(\pi - \theta_{knee})$$
$$\Rightarrow \theta_{knee} = \pi - \text{acos}(\vec{x}_{Thigh} \bullet \vec{x}_{Shank})$$

The results are as follows:

Table 1. Anatomical joint angles of the cat hindlimb in the default posture.

Default Posture:	
Hip angle	103.41°
Knee angle	94.29°
Ankle angle	100.38°

The range of the angles of most of the mechanical pin joints were determined by inspection on a decerebrate cat. The total range of motion of the mechanical joints from

the default posture has the following magnitudes in degrees: hip flexion-extension 60°, knee flexion-extension 65°; knee adduction-abduction 45°; ankle flexion-extension 85°; ankle adduction-abduction 30°.

2.3 Muscle Connections

2.3.1 Muscle Structure and Assumptions

SIMM uses the muscle architecture specified by the user and the Hill Model as default to compute the output files and necessary parameters for simulation. Muscle architecture parameters maximum tetanic tension, musculotendon length, fiber length, pennation angle (fiber angle), and physiological cross sectional area were taken from (Sacks and Roy, 1982). The maximum contraction velocities of the muscles were supplied by Dr. Burkholder. These parameters are summarized in Table 2.

Table 2: Muscle architecture parameters.

	Muscle name	Tension (N)	Lp (mm)	Lm (mm)	pen	PCA (cm2)	Vmax (cm/s)
ADF	Adductor femoris	102	69.5	62.6	0	4.48	63
ADL	Adductor longus	11.3	43.3	27.8	0	0.5	28
BFA	Biceps femoris anterior	47	84.6	34.5	14		36
BFP	Biceps femoris posterior	170	98.4	36.9	14	7.55	36
EDL	Ex digitorum	21.46	96.3	33.6	8	0.95	45
FDL	Flex digitorum	20.29	73.6	20.6	10	0.9	27
FHL	Flex hallicis	104.86	92	15.6	7	4.78	23
GMAX	Gluteus maximus	6	40.1	12	10		7
GMED	Gluteus medialis	60	40.1	12	10		7
GMIN	Gluteus minimus	4.21	40.1	11.9	10		7
GRAC	Gracilis	30.2	76.6	64.4	10	1.34	62
LG	Lateral gastrocnemius	102.9	95.4	24.5	17	4.58	32
MG	Medial gastrocnemius	90.16	90.4	20.9	21	4.01	23
PB	Peroneus brevis	33.5	73	8.8	0		9.7
PEC	Pectineus	10.6	28.3	21.1	0		15
PL	Peroneus longus	16.27	61.5	23.7	7	0.72	31
PLAN	Plantaris	76.8	97.7	18.7	14	3.41	18
PSOAS	Ilipsioas	122	94	19.2	0		19
PT	Peroneus Tertius	16	28.3	21.1	0	0.47	18
PYR	Pyrformis	26.1	29.3	11.6	5		7
QF	Quadratus Femoris	40.5	27.5	9.8	12		5
RF	Rectus Femoris	122	94.1	19.2	7	5.41	19
SART	Sartorius	20.1	144	105.5	0	0.89	101
SM	Semimembranosus	77.3	104.6	73.25	0	2.57	79
SOL	Soleus	20.48	84.7	41.7	7	0.91	24
ST	Semitendinosus	88.2	80.2	30.25	0	2.07	58
TA	Tibialis Anterior	26.17	89.4	52.2	7	1.16	69
TP	Tibialis Posterior	40.6	53.3	8.4	14	1.8	8
VI	Vastus Intermedius	40.8	83.7	22.6	7	1.81	22
VL	Vastus Lateralis	147	90.4	27.3	17	6.5	26
VM	Vastus Medialis	61.1	85.1	26.9	17	2.71	26

SIMM has the ability to extract the output parameters such as muscle orientation, tendon strain, muscle force, fiber length, moment arms, and musculotendon length subject to different postures. Some of the output parameters were exploited for torque calculations (Section 3.3.1) and validation purposes (Section 2.4), and others can be used for further analysis.

2.3.2 Muscles

The muscle file was created by appropriate conversion of the muscle data from the DADS model to the SIMM model. The muscle geometry was assumed to be a line or lines attached end to end between the connection points to the hindlimb. Each muscle contains at least two connection points to the bones neighboring the joint it spans. SIMM requires the information of muscle connection points to the bones in LCS of the corresponding bone. The transformation of the connection points among the two models was done similar to the procedure followed in joint files, except there is a translation of the data from the Muscle CS to the CSYS CS of the corresponding segment.

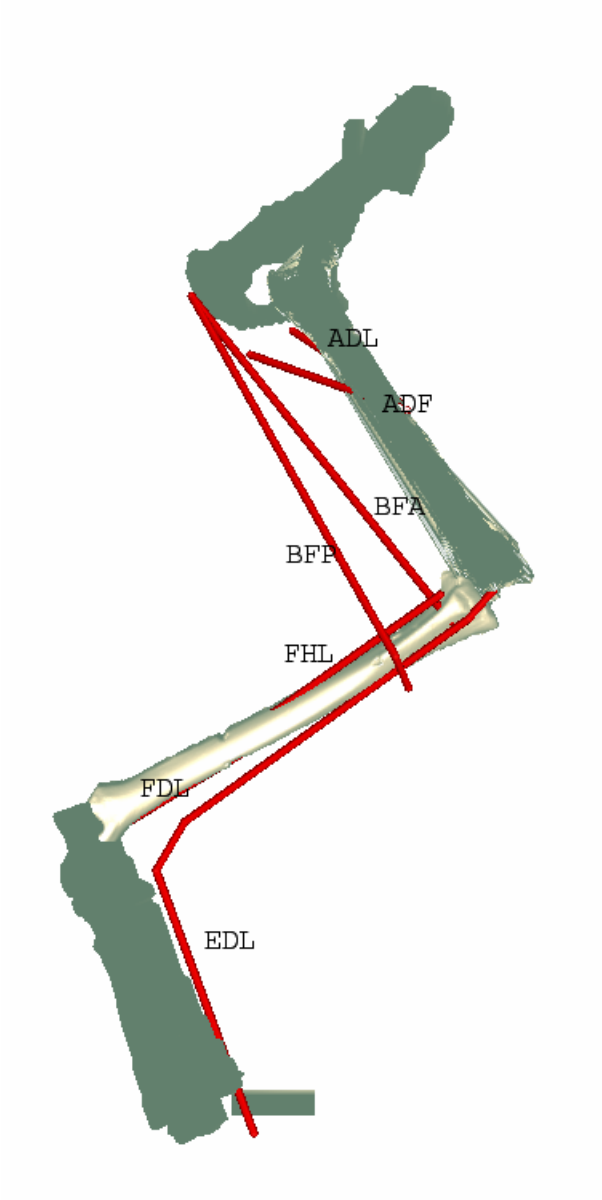

Figure 8: Representation of muscles as lines attached to the bones or connective tissue in SIMM. See Table 2 for abbreviations.

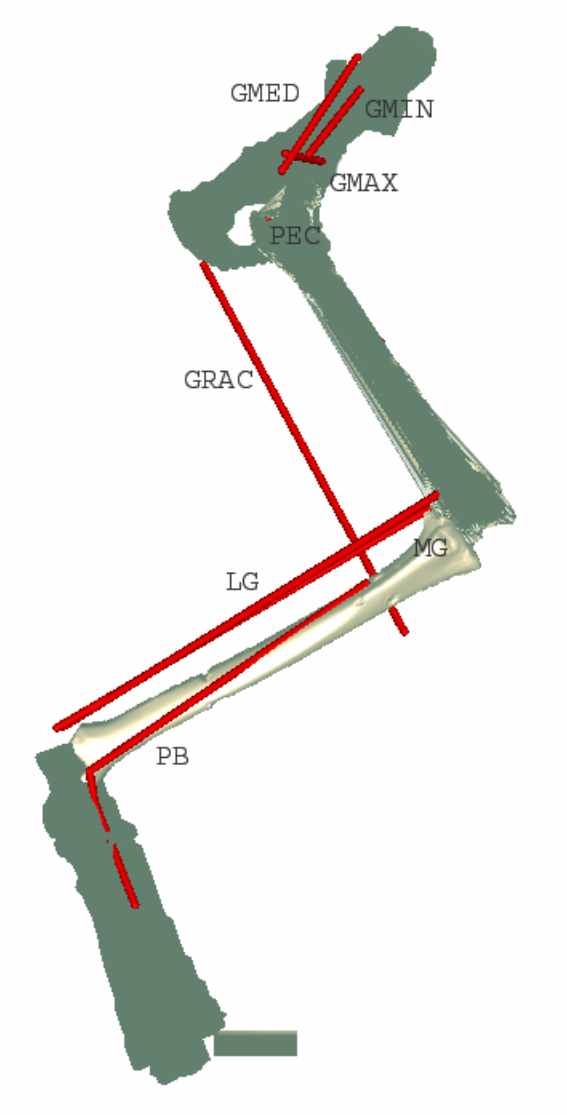

Figure 9: Representation of muscles in SIMM model.

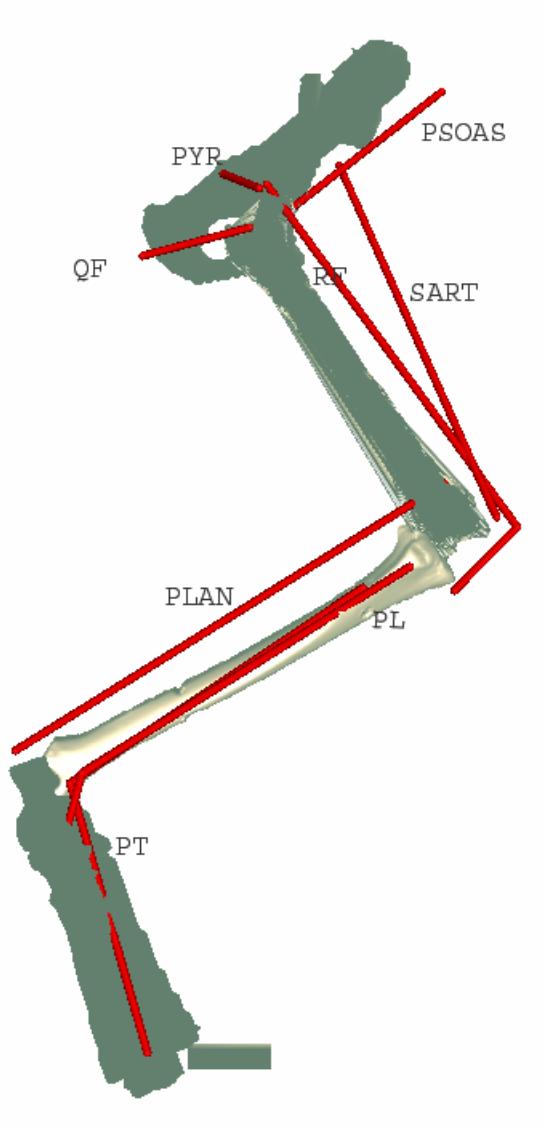

Figure 10: Representation of muscles in SIMM model.

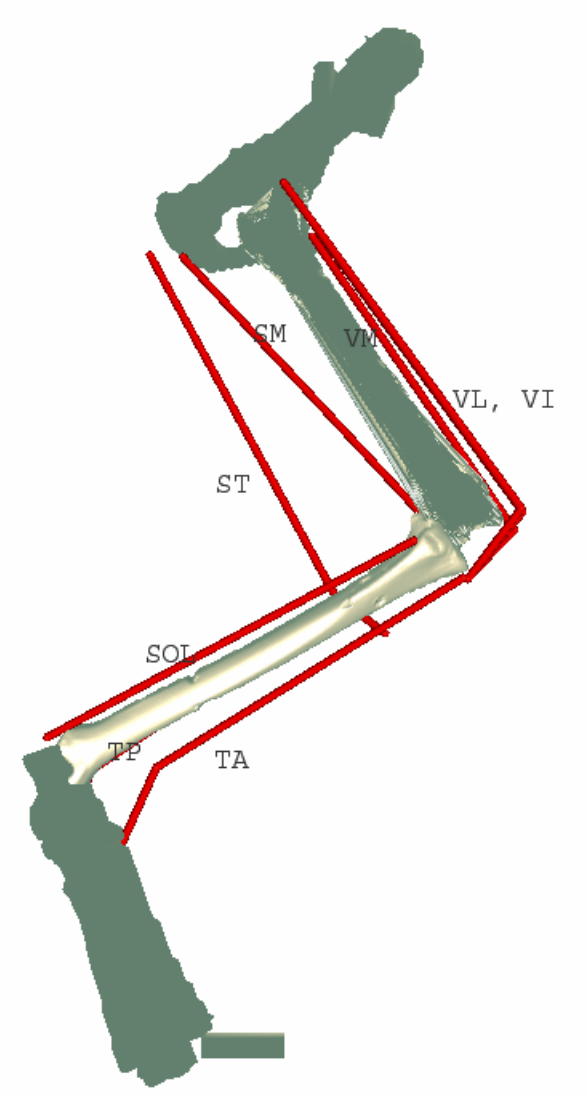

Figure 11: Representation of muscles in SIMM model.

By glancing at Figure 8-11, one can perceive how muscles are idealized. Muscle connection points are divided into three groups: origins, via points and insertions. The proximal bony attachment site is called origin and the distal attachment site is called insertion. The via points define the turning points around the bones to match the physiological moment arms. For example, the vasti muscles start at the anterior part of the femur bone and terminate at the upper anterior part of the tibia bone. The via point is

added into the muscle file such that it changes the direction of the muscle and wraps it around the patella (knee cap). Some muscles have up to five connection points.

2.3.3 Thigh Muscles Example

The procedure of the muscle data calculation of the femur in SIMM is demonstrated. The origin of a thigh muscle in Thigh Muscle CS was transformed to the LCS of the femur according to the hierarchy shown in Figure 4. The muscle point vector in Thigh Muscle CS, V_{Thigh} , is represented in Figure 12 as the green dashed line. We calculated V_{Thigh} in LCS of the femur bone ($V_{femurLCS}$, which is black dashed line).

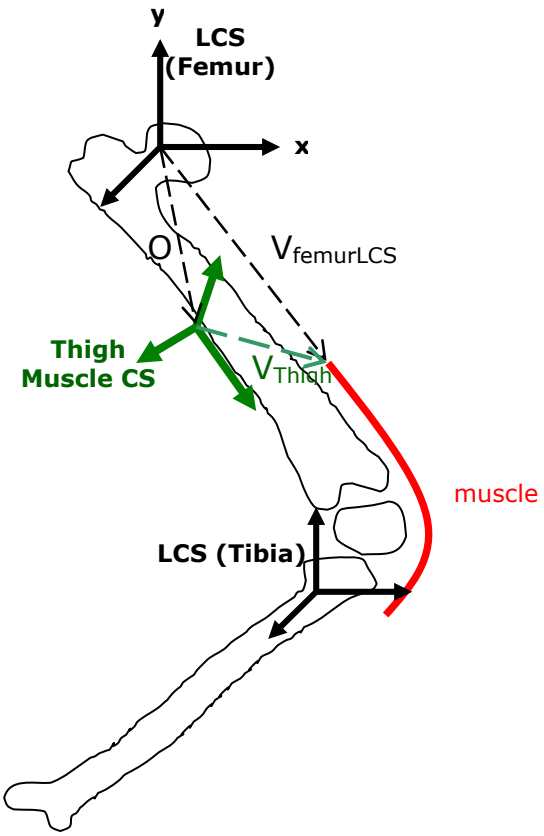

Figure 12: A sketch for the calculation of muscle connection points to the thigh.

$$R_{femur} = R_{femurLCS}^{World} \cdot R_{World}^{ThighSYS}$$

$$V_{femurLCS} = R_{femur} \cdot (R_{ThighSYS}^{Thigh} \cdot V_{Thigh} + O_{Thigh}^{ThighSYS})$$

The coordinate transformation of V_{Thigh} vector was done by translation and using the rotation matrices. First, V_{Thigh} is rotated into ThighSYS CS, whose origin is the femur LCS. The origin vector of Thigh CS shown as the black dashed arrow O in Figure 12 is in ThighSYS CS. Since these two vectors (V_{Thigh} and O) are in the same CS (ThighSYS) we can add them. The resultant vector is rotated by R_{femur} (also used in the joint file explanation above) representing the rotation matrix from ThighSYS to femur LCS.

The MATLAB file 'muscle.m' was created to code all muscle connection points into the SIMM muscle file, automatically. Via points are calculated in the same way using the MATLAB file 'ViaPoints.m' and placed in the SIMM muscle file manually.

2.4 Validation of the SIMM Model

Comparisons of the muscle lengths and muscle moment arms were made between the two models to validate the SIMM model. This validation allowed us to have confidence in the many coordinate transformations that were required for generating the SIMM model from the DADS model. Muscle lengths calculated from the DADS model were very similar to the SIMM values. On the other hand, some of the moment arms did not match between the two models.

Another comparison could be the direction of the end point forces produced by the hindlimb. Directional forces of single muscles in the static posture is tabulated in Section 4.1.2. Since the femur is fixed in the DADS model, the effect of the hip could not be taken into account in this analysis.

Figure 13 shows a lateral view of the SIMM model in the General Coordinate System (GCS). x is in the anterior direction, y is in the negative gravity direction and z is in the lateral direction pointing out of the page for all the bones. The posture was determined by the hip, knee and ankle angles, which are 103.41, 94.29 and 100.38, sequentially. Alignment of the LCS occurs only for this particular posture of the right hindlimb. Red lines represent all the muscles modeled.

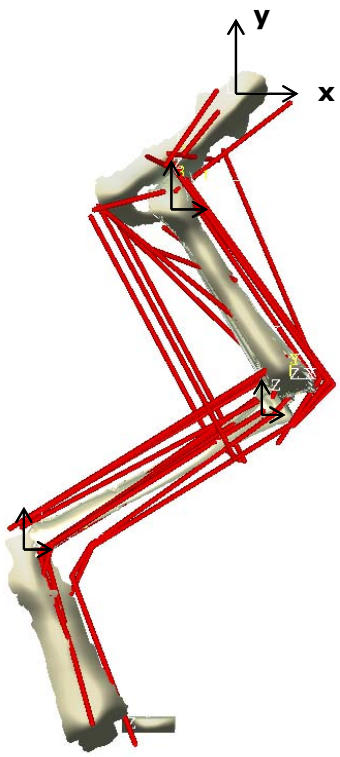

Figure 13: Lateral view of the SIMM model in the General Coordinate System (GCS).

2.4.1 Muscle Length Comparison

Comparing muscle lengths in the two models is a reasonable way to examine similarity between them. The length of a vector does not change whatever reference frame it is defined in. The muscle connection points, which can be thought as the beginning and end points of a vector, are in different coordinate systems in SIMM and DADS. In the SIMM muscle file, all the muscle connection points are in the related segment's Local Coordinate System (LCS). The coordinate axes of the LCS are parallel to the GCS axes

in the default posture. On the other hand, in the DADS model, the muscle connection points are expressed in different CSs such as Pelvis, Thigh, Shank and Foot in Figure 4, depending on the segment to which the muscle is attached. The x axes of these coordinate systems are aligned with the longitudinal orientation of the bones.

SIMM muscle lengths are calculated using the 'Plot Maker' editor in the software. Plot Maker can calculate the changing musculotendon lengths with respect to the joint angles. The muscle lengths in DADS were provided by Dr. Burkholder.

In its procedure for calculating muscle lengths, DADS does not take into account the parts of muscles that do not contract, i.e. those connected to the same bone. Non-contracting parts of the muscles were calculated and added to match the results of SIMM. The muscle lengths shown in Figure 14 in both of the models are tabulated in Table 3. The detailed calculations can be found in the MATLAB file "noncontractingLengths.m." The muscle that has the maximum difference between the two models is Tibialis Posterior (TP) (1.03% length change of DADS TP length). This small percentage validates the proposition that SIMM and DADS models are the similar.

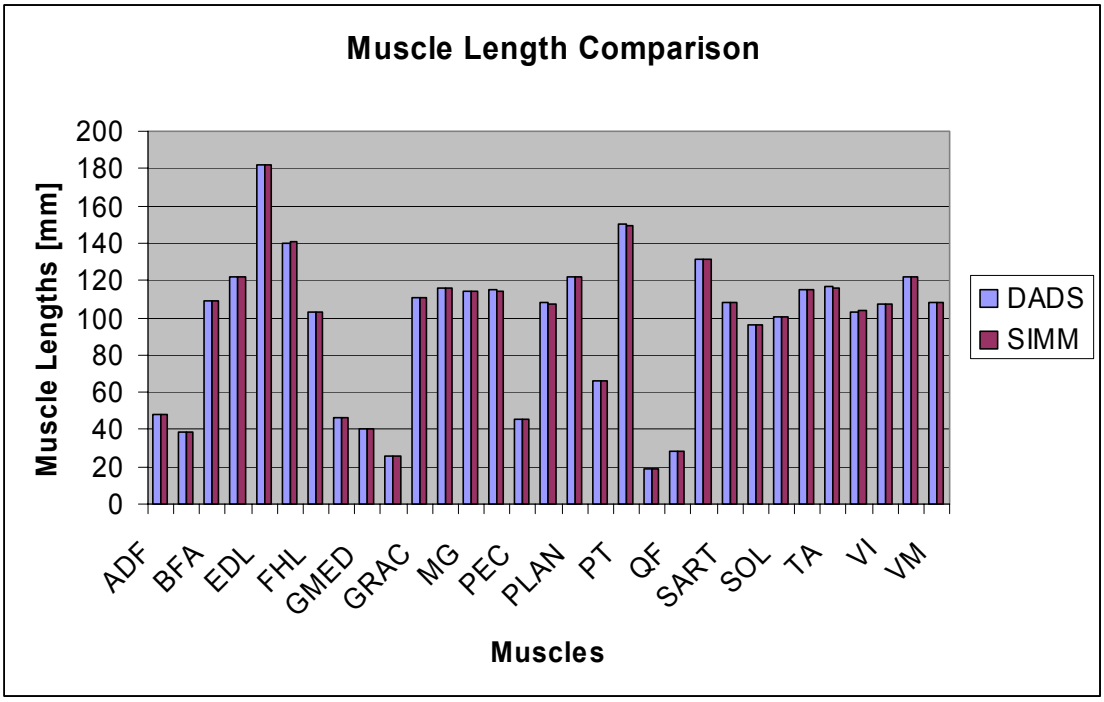

Figure 14: Comparison of muscle lengths of the SIMM model (red) and DADS (Burkholder model) (blue).

Table 3: Muscle Length Comparison between the models constructed in SIMM and DADS (Burkholder model).

Muscle Lengths(mm)	connection points	DADS	noncontract. in SIMM	Adjusted DADS	SIMM	segment noncontrac.
ADF	p.fe	47.92		47.92	47.92	
ADL	p.fe	38.21		38.21	38.21	
BFA	p.fe	109.35		109.35	109.35	
BFP	p.t.t	111.12	10.68	121.80	121.80	tibia
EDL	fe.t.t.fo.fo	29.29	152.48	181.77	181.73	tibia+foot
FDL	t.t.fo.fo	14.45	125.22	139.67	140.70	tibia+foot
FHL	t.fo	103.33		103.33	103.34	
GMAX	p.fe	46.65		46.65	46.65	
GMED	p.fe	40.31		40.31	40.31	
GMIN	p.fe	25.41		25.41	25.41	
GRAC	p.t	110.31		110.31	110.31	
LG	fe.fo	115.47		115.47	115.77	
MG	fe.fo	113.96		113.96	114.11	
PB	t.t.fo.fo	7.84	107.01	114.84	114.06	tibia+foot
PEC	p.fe	45.90		45.90	45.90	
PL	t.t.fo	15.86	92.26	108.12	107.28	tibia
PLAN	fe.fo	121.72		121.72	122.04	
PSOAS	p.fe	66.32		66.32	66.32	
PT	t.t.fo	65.75	84.13	149.88	149.26	tibia
PYR	p.fe	18.78		18.78	18.78	
QF	p.fe	28.17		28.17	28.17	
RF	p.fe.t	131.09		131.09	131.09	
SART	p.fe	108.44		108.44	108.44	
SM	p.t	96.17		96.17	96.17	
SOL	t.fo	100.33		100.33	100.60	
ST	p.t.t	99.22	16.11	115.33	115.33	tibia
TA	t.t.fo	29.44	87.19	116.63	116.08	tibia
TP	t.t.fo	12.77	90.10	102.88	103.94	tibia
VI	fe.fe.t	21.09	86.59	107.68	107.68	femur
VL	fe.fe.t	21.47	100.50	121.96	121.96	femur
VM	fe.fe.t	17.55	90.85	108.40	108.40	femur

2.4.2 Validation of Moment Arms

The moment arm of a muscle is a crucial factor in determining the joint torque. The moment arm of a muscle at a joint is the shortest perpendicular distance from the line of pull of the muscle to the joint axis. A conceptual diagram of a moment arm of a biceps muscle is shown below in Figure 15:

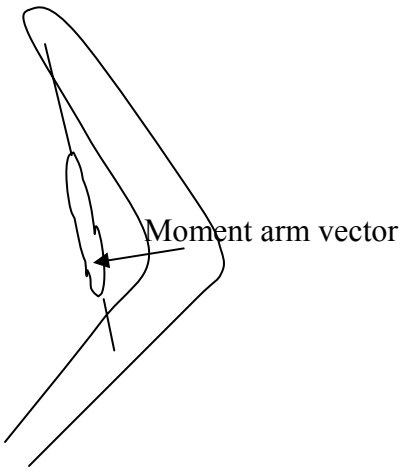

Figure 15: A representation of a biceps muscle moment arm.

There are different experimental methods for calculation of the instantaneous moment arms. One method is to calculate the change of length of the muscle tendon divided by the incremental change of the joint angle. Another method is to measure the joint torque and examine the mechanical advantage of the moment arm. Some moment arms (adduction-abduction and inversion-eversion) change sign as the joint angle changes (Young et al., 1992). For example, tibialis anterior, which is located at the anterior part of the tibia and foot, stabilizes the foot joint by switching from abductor to adductor or vice verse. Therefore, joint axis and moment arm determinations are important.

Some of the moment arms of the Burkholder hindlimb model (DADS model) and the SIMM model were different. Table 3 demonstrates the moment arms in the two models and the differences as a percentage of Burkholder moment arms. In the former, the moment arms were calculated from segmental motion and muscle excursion. In the latter, the plot maker editor of SIMM was utilized to extract moment arms for the default posture, as is explained in Section 3.3.1. Hip moment arms could not be compared because those values were not available in the previous model. Since the moment arms of Dr. Burkholder's model are similar to the literature values (Young et al., 1992, 1993), the SIMM model is a reasonable source for further calculations like force and moment.

Table 4: Muscle moment arm comparison with the Burkholder model (DADS model).

	Knee ext.		Differ.	**Knee ad.**		Differ.	**Ankle ext.**		Differ.	**Ankle ad.**		Differ.
Muscl.	**Burk.**	**SIMM**	%	**Burk.**	**SIMM**	%	**Burk.**	**SIMM**	%	**Burk.**	**SIMM**	%
BFP	-27.8	-31.5	13%	19.6	13.3	32%						
EDL	2.7	2.7	0%	-2.7	-3.4	26%	-10.9	-12	10%	3.2	-0.1	103%
FDL							2.2	1.8	18%	8.5	8.3	2%
FHL							2.3	2.6	13%	-0.8	-0.1	88%
GRAC	-28.2	-28.1	0%	-11	-2.1	81%						
LG	-8.8	-8.3	6%	-11.8	-4.9	58%	15	15	0%	-1	2.4	340%
MG	-8.6	-8.9	3%	0.6	1.3	117%	15.7	15.7	0%	-2.2	1.3	159%
PB							0.2	0.4	100%	-5.6	-5.6	0%
PL							-2.1	-2.1	0%	-5.7	-6.2	9%
PLAN	-9.4	-8.8	6%	-13.3	-5.6	58%	15.5	15.7	1%	-0.9	2.6	389%
PT							-1.8	-1.6	11%	-3.8	-4.4	16%
RF	10.5	10.4	1%	5.7	-0.9	116%						
SM	-6.7	-5	25%	-12.2	-5.6	54%						
SOL							13.5	13.6	1%	-0.9	2.2	344%
ST	-36.5	-35.5	3%	-8.2	-3.5	57%						
TA							-15	-14.8	1%	0.1	-3.8	3900%
TP							-0.5	-0.8	60%	9.3	8.6	8%
VI	9.8	9.5	3%	8.3	0.6	93%						
VL	9.5	9.1	4%	10.5	1.9	82%						
VM	9.8	9.9	1%	1.1	-3.4	409%						

The flexion- extension axis moment arms of SIMM are quite similar to Dr. Burkholder's model. However, the adduction axis moment arms were much less similar. Flexion-extension moments change the same amount as adductor-abductor moment arms among different postures.

III. THE JACOBIAN MODEL

In order to compute the endpoint force system from a set of muscle activations, the hip rotation axis was omitted from the Jacobian and force analysis so that an invertible Jacobian matrix could be obtained. Originally the SIMM feline hindlimb model had seven mechanical degrees of freedom.

3.1 Model Development

We derived a Jacobian from the SIMM model to understand the mapping between the muscle activations and the ground-reaction force at the toe in a static posture. The Jacobian method (Zatsiorsky, 2002) is typically used to find the forces and moments generated by a linkage system when known joint torques are applied. We then used the Jacobian to understand how multiple muscles generating torques at each joint contributed to the end point force.

3.1.1 Overview of the Force Transformations

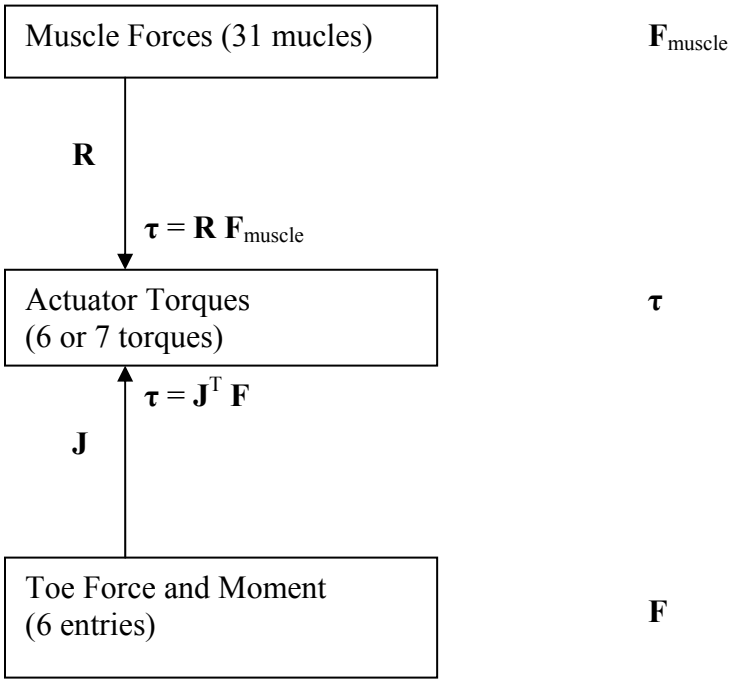

Figure 16: Overview of all the force transformation computations.

All the force transformations between the muscles, joint torques and end point were broken up into two transformations as in Figure 16. The joint torque vector ($\boldsymbol{\tau}$) is the projection of the muscle forces onto 6 or 7 joints. The discussion about the number of joints in the analysis is given in Section 3.1.3. The muscle force projection was performed using a moment arm matrix (**R**). The transformation into joint torques from the end point force and moment space (**F**) was performed using the Jacobian matrix (**J**). The Jacobian matrix is explained in Sections 3.1.2 and 3.1.3.

3.1.2 The Jacobian Matrix

The Jacobian matrix is the mechanical mapping between joint torques, force, and moment applied by the system at a given point. In a musculoskeletal system, the torque at a mechanical joint is generated by the muscles crossing it (Section 3.3.1). Joint torques are calculated by multiplying the transpose of the Jacobian by the end-effector force system.

$$\boldsymbol{\tau} = \mathbf{J}^{\mathrm{T}}\,\mathbf{F}$$

where, τ: Joint torques (7x1)

J: Jacobian (6x7)

F: end-effector force system (6x1)

The end-effector force system is the 6x1 vector whose upper half is composed of the force values in x y and z directions, and whose lower half is the moment values in x y and z directions of the Global Coordinate System (GCS). These values are the resultant force and couple applied by the toe to the ground.

The Jacobian can be computed from the position vectors, r, from the end point (toe) to the joint axes, and the joint axis direction vectors, z (Sciavicco and Siciliano 2000; Paul, 1981).

$$\begin{bmatrix} \tau_1 \\ \vdots \\ \tau_n \end{bmatrix} = \begin{bmatrix} \mathbf{r}_{e,1}\times\mathbf{z}_0 & \cdots & \mathbf{r}_{e,j}\times\mathbf{z}_{j-1} & \cdots & \mathbf{r}_{e,n}\times\mathbf{z}_{n-1} \\ \mathbf{z}_0 & \cdots & \mathbf{z}_{j-1} & \cdots & \mathbf{z}_{n-1} \end{bmatrix}^T \begin{bmatrix} \mathbf{f} \\ m_e \end{bmatrix}$$

The Jacobian matrix changes with posture because the values of the r and z vectors change. We computed the Jacobian for a posture of 103, 94, 100 degrees of anatomical hip, knee and ankle angles, respectively. Below (Figure 17) is a sketch of the open kinematic chain composed of the bones, the position vectors and the joint vectors of the hindlimb.

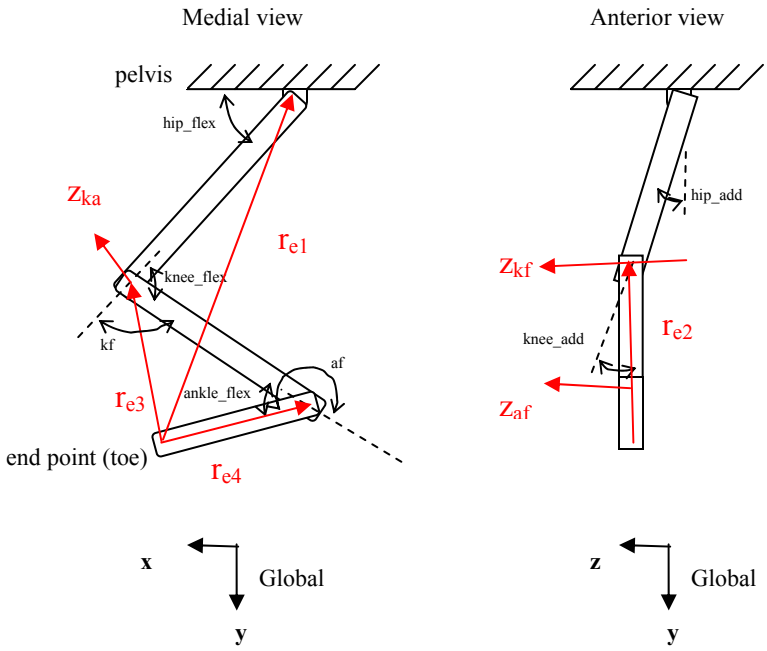

Figure 17: A sketch of the open kinematic chain composed of the bones, the position vectors and the joint vectors of the hindlimb.

3.1.3 Inverse Jacobian and Model Simplification

Taking all seven joints into account, the Jacobian matrix would be 6x7. In this case, there is the joint redundancy and the inverse of the Jacobian is not defined. In fact, the

problem is over determined, and so for an arbitrary joint torque vector there is no solution for end point force and moment.

The equation involving our non-invertible Jacobian matrix was solved by decreasing the degrees of freedom of the system by one. The translations and rotations of some of the joints were already ignored in the seven d.o.f. SIMM model, earlier. In addition, here the hip internal-external rotation was omitted since it has a small range of motion. The validity of this simplification is discussed in Section 3.3.2. The size of the Jacobian matrix was decreased by one column to 6x6. The column vectors of the 6x6 Jacobian were independent and the null space was empty. Since it had the rank of six, it was invertible.

Thus, in Figure 16 the transformation at the bottom can now be performed in both directions, i.e.:

$\boldsymbol{\tau} = \mathbf{J}^{T}\,\mathbf{F}$

and $\mathbf{F} = \mathbf{J}^{-T}\,\boldsymbol{\tau}$

Now that the matrix is invertible, the problem is similar to biomechanics problems discussed in the literature. For example, the Jacobian is inverted by Valero-Cuevas et al. (2003, 1998), Spagele et al. (1999), Tarchandis et al. (1995), and Pollard and Gilbert (2002). In all of these studies the degree of freedom of the system is equal to the dimension of the end point force vector (5 d.o.f. human thumb, 4 d.o.f. human index finger, 3 d.o.f. human leg, and 4 d.o.f robotic finger) and the Jacobian matrix is

invertible.

The Jacobian matrix that will be used in the force analysis for six d.o.f. is:

$$J_{6x6} = \begin{bmatrix} r_{e1} \times z_{hf} & r_{e1} \times z_{ha} & r_{e2} \times z_{ke} & r_{e3} \times z_{ka} & r_{e4} \times z_{ae} & r_{e5} \times z_{aa} \\ z_{hf} & z_{ha} & z_{ke} & z_{ka} & z_{ae} & z_{aa} \end{bmatrix}_{6x6}$$

r: position vector from toe to the segment origin on the related rotation axis. The letter e in the subscript refers to end point toe, the numbers refer to joints. 1: hip flexion, hip adduction, 2: knee extension, 3: knee adduction, 4: ankle extension, 5: ankle adduction.

z: rotation axis vector in global coordinate system (GCS).

hf: hip flexion, ha: hip adduction, ke: knee extension, ka: knee adduction, ae: ankle extension, and aa: ankle adduction.

3.2 Validation of 6 DOF Jacobian

The Jacobian in the static analysis was verified for consistency in a velocity analysis. Force-velocity duality (Craig, 1986) allows us to use the same Jacobian matrix in both static and kinematic analysis. Therefore, the Jacobian computed in the static analysis was plugged in a velocity equation. Incremental end point position change vectors were calculated from the velocity equation and also from a graphical tool in SIMM. The position vectors were compared.

3.2.1 Velocity Analysis

The Jacobian matrix also maps the joint angular velocities to linear velocities. The Jacobian for a system at a certain posture should satisfy both the static force equations and the velocity equations.

According to velocity analysis, the linear and angular velocity vector (6x1) of the end point (toe) is equal to the Jacobian (6x6) times the angular velocity (rate of change of joint angles) vector (6x1).

$$\begin{bmatrix} \vec{v} \\ \vec{\omega} \end{bmatrix} = J \cdot \dot{\vec{\Theta}}$$

The above linear relationship can be approximated by differential angle and position changes (Ebert-Uphoff and Kozak, 2002).

$$\begin{bmatrix} \Delta\vec{p} \\ \Delta\vec{\varphi} \end{bmatrix} = \begin{bmatrix} 1 & 0 \\ 0 & B(\varphi) \end{bmatrix} \cdot J \cdot \Delta\vec{\Theta}$$

The upper half of the Jacobian was validated:

$$\Delta\vec{p} = J_{upper} \cdot \Delta\vec{\Theta}$$

The upper half involves the cross product of joint center position and joint axis vectors, whereas lower half involves only the joint axis vectors. Therefore, the validation of the upper half is satisfactory.

For convenience, the Jacobian matrix calculated in the static analysis in Section 3.1.2 was substituted into the velocity analysis ($\Delta\vec{p} = J_{upper} \cdot \Delta\vec{\Theta}$). Differential linear position change of the end point, $\Delta\vec{p}$, was obtained by multiplying the Jacobian determined in the static analysis by the vector of incremental change in the joint angles, $\Delta\vec{\theta}$, in radians. This was done for three cases:

1° increment of hip flexion joint angle,

1° increment of knee extension joint angle,

and 1° increment of all the joint angles.

3.2.2 The SIMM Marker Editor

A graphical tool in SIMM, the Marker Editor, was used to calculate the differential position change subject to the joint angular change for comparison of the results of the velocity analysis. The default toe point was marked as offset point. Joint angles were changed incrementally such that in the first case, the hip flexion joint angle was increased 1°. Corresponding incremental positional vector change $\Delta\vec{p}_{Target}$ was noted, which is the target of the Jacobian velocity analysis. In the second case, the knee extension joint angle was increased by 1° and in the third case, all the joint angles were increased by 1° and corresponding $\Delta\vec{p}_{Target}$ values were noted.

3.2.3 Comparison of the SIMM Model and Velocity Analysis

To verify the Jacobian calculated in the static analysis, error in the velocity analysis was computed. The end point positional change vector, that is, the target vector, determined by the SIMM marker editor and the same vector estimated in the velocity analysis were compared by calculating the distance between the end points of these two vectors. This distance gives the length of the error vector shown in Figure 18.

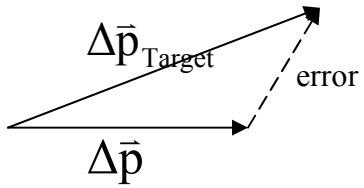

Figure 18: Representation of the error vector between the incremental end point position change found by SIMM Marker Editor (ΔpTarget) and velocity analysis of Jacobian (Δp).

Cosine theorem and dot product were utilized in the calculation of the length of the error vector.

$$\text{error}^2 = \left|\Delta\vec{p} - \Delta\vec{p}_{Target}\right|^2$$
$$= (\Delta\vec{p} - \Delta\vec{p}_{Target})^T(\Delta\vec{p} - \Delta\vec{p}_{Target})$$
$$= \Delta\vec{p}\cdot\Delta\vec{p} + \Delta\vec{p}_{Target}\cdot\Delta\vec{p}_{Target} - 2\Delta\vec{p}\cdot\Delta\vec{p}_{Target}$$

The length of the error vector divided by the length of the target vector allows us to compare the results in different set of incremental joint angle changes.

$$\%\text{error} = \text{error} \div \left|\Delta\vec{p}_{\text{Target}}\right| \cdot 100$$

The MATLAB file "JacobianValidation.m" was created for calculating the end point position change and the percentage error in the velocity analysis.

Table 5: Comparison of the Incremental End Point Change in SIMM and in Jacobian Velocity Analysis.

Angle Change	$\Delta\vec{p}$ components* incremental end point position change	Target (from SIMM Model)	Validation $J \cdot \Delta\vec{\Theta}$	Error (% of Target)
Hip flexion	x:	3.6819	3.6795	0.8728%
changed by 1°	y:	-0.2742	-0.3063	
	z:	0	0	
Knee extension	x:	2.1650	2.1556	0.8726%
changed by 1°	y:	-1.0121	-1.0305	
	z:	0.3867	0.3913	
All angles	x:	5.0742	5.0183	1.9848%
changed by 1°	y:	-2.3209	-2.4275	
	z:	-4.1286	-4.0616	

In Table 5 and Figure 19 the percentage error is demonstrated for three different sets of incremental joint angle changes: hip flexion joint angle change, knee extension joint angle change and angular change of all the joints. The error corresponding to 1° change of hip flexion joint angle is almost the same as the error corresponding to 1° change of

knee extension joint angle. On the other hand, when all the joint angles are changed by 1°, the percentage error increases as expected. According to the percentage error values, we can conclude that the Jacobian matrix used in the static analysis is accurate except that it does not take the effect of seventh joint into account.

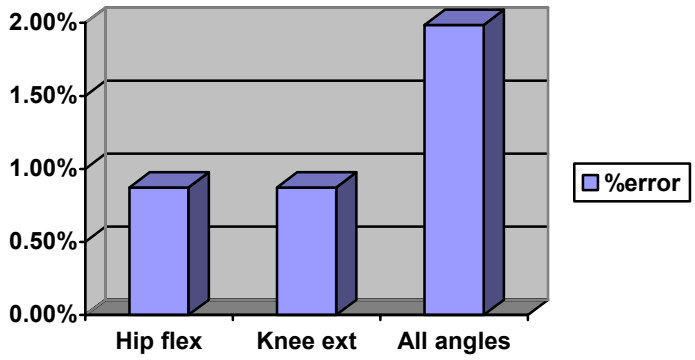

Figure 19: The deviation of the velocity analysis from the SIMM 'Marker Editor' values for three different cases of incremental joint angle changes.

3.3 Torque Generation

3.3.1 Moment Arm Recruitment

As a second step in the calculation of the end effector force, the joint torques were calculated as a function of individual muscle activations after computing the Jacobian matrix. Muscle forces and moment arms determine joint torques.

$$\boldsymbol{\tau}=\mathbf{R}\mathbf{F}_{\mathbf{muscle}}$$

where **R** is the 6x31 moment arm matrix

$\mathbf{F}_{\mathbf{muscle}}$ is the 31x1 isometric muscle force vector.

Each column of **R** corresponds to a muscle and each row corresponds to a mechanical joint. Each row of $\mathbf{F}_{\mathbf{muscle}}$ gives the force generated by a muscle. It is the maximum force that a particular muscle can generate scaled by the activation level e ($0 \leq e_i \leq 1$) (Zajac, 1989):

$$\mathbf{F}_{\mathbf{muscle}} = \mathbf{F}_{\mathbf{max}}\mathbf{e}.$$

$\mathbf{F}_{\mathbf{max}}$ is a 31x31 diagonal matrix with maximum muscle force values on the diagonal (See Table 2 for tabulated values). The maximum force that a muscle applies depends on its physiological cross sectional area (PCSA) (He et al., 1991):

$$F_{max} = PCSA.\sigma.g$$

where σ (specific tension) times g (gravity) is the maximal muscle stress ($=[2.3kg/cm^2][9.81kgm/s^2]$) (Spector et al., 1980).

Pennation angles of the muscles (the orientation of the muscle fibers along the line of action of the muscle) are assumed to be low enough not to affect maximum muscle force (less than 10°).

Finally, the static force equation becomes:

$\mathbf{F}=\mathbf{J}^{-T}\mathbf{R}\mathbf{F}_{max}\mathbf{e}$ (Valero-Cuevas, 1998)

The above equation is the linkage between the muscle activations ($\mathbf{e}_{31x1}$) and the end-effector force system ($\mathbf{F}_{6x1}$). It is utilized in the transformation of single muscle forces at the end effector, finding the feasible end point force set, and the maximum end point force. The term $\mathbf{J}^{-T}\mathbf{R}\mathbf{F}_{max}$ is constant for a certain posture of the hindlimb. It is a 6x31 non-invertible matrix, that is, there is a many to one relationship between the end point force system and the muscle activation pattern. The same end point force and couple can be generated by different combinations of muscle activations. There are many posture dependent, and estimated anatomical parameters in the constant term such as: 5 position vectors, 6 joint axis vectors, 186 moment arms (31 muscles x 6 DOFs), and 31 muscle cross section areas.

3.3.2 Torque Analysis at the Omitted Joint

Validity of the omitted hip internal-external rotation axis in the Jacobian analysis was investigated using the following procedure:

1) First, an activation pattern, e, was selected and the analysis was performed as before omitting the 7th joint, i.e. using the 6x6 Jacobian matrix. The 6-dimensional torque vector, $\boldsymbol{\tau}$, and the 6-dimensional force-moment vector, **F**, were thus calculated.

2) Then the joint torques of the omitted joint were calculated in two different ways:

a) From the actuation pattern, **e**, all 7 components of the torque vector, τ_7, were calculated. This provides the correct value for τ_7.

b) From the force-moment vector, **F**, calculated with the omitted joint, the 6x7 Jacobian was used to also calculate a 7-dimensional torque vector.

The first 6 components of the τ vector calculated in Steps 2a) and 2b) were guaranteed to be identical. Ideally, the seventh joint torque value would also be identical, indicating that the omission of the seventh joint did not affect the force-moment combination **F**. Thus, the difference between the two values obtained for τ_7 and Steps 2a) and 2b) provide a measure for how significantly the seventh joint affects the resulting force-moment F.

The above procedure was executed for two different activation patterns. The results are shown in Table 6.

Interpretation of results: As seen in Table 6, the results for τ_7, differed somewhat (30% relative error) for the first case, but more significantly for the second case (90% relative error). These results indicated that it would be very valuable for future research to refine the model provided in this thesis to also include the seventh joint.

Table 6: Validation of the omitted hip internal-external rotation axis.

Activation pattern 1	**e** = [1.0 0.0 0.0 0.3 0.0 0.0 1.0 0.0 1.0 0.0 0.0 1.0 1.0 0.0 0.0 0.0 0.3 0.0 0.0 0.0 0.0 1.0 0.0 1.0 1.0 0.0 0.0 0.0 0.0 1.0 0.0]^T **F** = [-34.15 -50.78 3.55 0 0 0]^T (**J**$_{6x6}$ used)		
	τ (Torques from **e**)	**τ** (Torques from **F**) (**J**$_{6x7}$ used)	Difference:
Hip flex	-6.3071	-6.3074	
Hip add	0.4474	0.4475	
Hip int-ext	-1.0610	-0.7413	30 %
Knee exten	-1.1392	-1.1395	
Knee add	-0.1099	-0.1098	
Ankle exten	3.8137	3.8137	
Ankle add	0.4567	0.4567	
Activation pattern 2	**e** = [1 0 0 1 0 0 0 0 1 0 0 0 0 0 0 0 0 0 0 0 0 1 0 1 0 0 1 0 0 1 0]^T **F** = [-79.18 -22.61 1.57 0.67 -2.70 6.25]^T (**J**$_{6x6}$ used)		
Hip flex	-10.0418	-10.0418	
Hip add	0.8731	0.8731	
Hip int-ext	-2.3791	-4.5401	90 %
Knee exten	-3.1298	-3.1298	
Knee add	1.9972	1.9972	
Ankle exten	-0.3869	-0.3869	
Ankle add	-0.0983	-0.0983	

3.3.3 Biarticular Muscles and Free Body Diagram

The multiarticular muscles can be modeled as the combinations of uniarticular muscles as long as this does not change the joint torque application of uniarticular muscles. Muscles spanning a number of anatomical joints are called multiarticular. To name a few, biceps, gastrocnemius, extensor digitorum longus, etc. Biarticular muscles cross two anatomical joints.

The effect of a multiarticular muscle around each joint it spans is independent of the effect on other joints. Thus, in the torque equation of the muscles, a multiarticular muscle can be treated as a combination of uniarticular muscles with the same muscle force. The moment arms of the corresponding uniarticular muscles are the same as the multiarticular one.

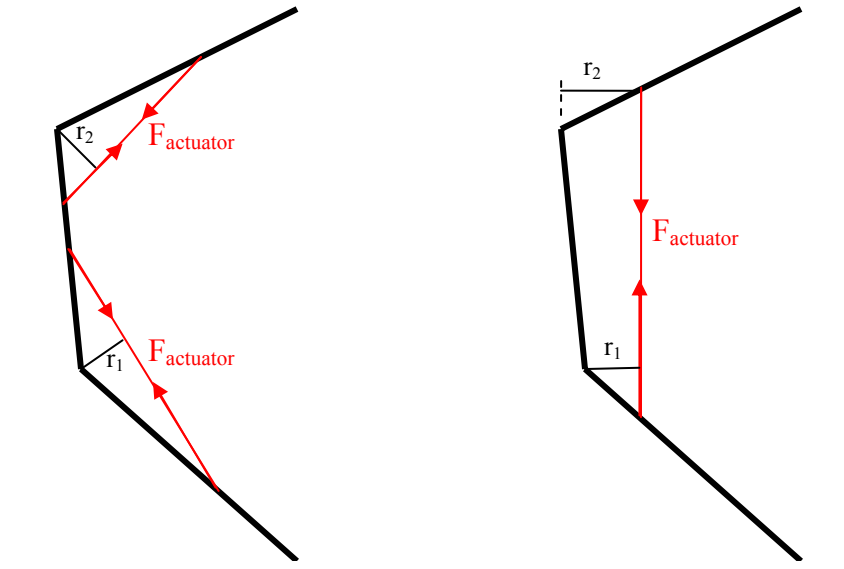

Two uniarticular muscles A biarticular muscle

Figure 20: Sketches of two uniarticular muscles and a biarticular muscle.

Specifically, joint torques applied by a biarticular muscle are equal to the torques of two uniarticular muscles having the same muscle force and the same moment arms around the joints (Figure 20). Free body diagrams of a biarticular muscle and two uniarticular muscles were drawn in a simplified three link system. The link connections were pin joints. Joints were assumed to be stiff so that the system did not collapse unless a torque is applied around the joints. Given an end point force and moment, the joint torques were compared in the static equilibrium for biarticular muscle and uniarticular muscles. Both biarticular muscle and uni-articular muscles were subject to the same contraction force and had the same moment arms around the two pin joints: r_1 and r_2. As a result, in both circumstances the joint torques were equivalent. On the other hand, the joint forces were different.

In the current analysis, joint forces were not taken into account; since their effect is compensated by the inherent joint properties (i.e. pin joint only allows rotation). In other words, the joint forces intersect with the joint axes and they do not apply torque around the joint.

Studies on models of the human and animal hindlimbs in the literature support the idea that force components of biarticular muscles due to their action around spanned joints can be added as a vector sum. Moreover, the action of more than one uniarticular muscle can be found by vectorial addition of the participating muscles in terms of force (Hof, 2001; Yamaguchi, 2001).

IV. FORCE ANALYSIS

A static end point force system was calculated for each individual muscle and various muscle activation patterns. This way the role of individual muscle actions in the "force constraint strategy" can be understood. The effect of individual muscles torques transmitted to the end-effector was compared to experimental values (Murinas 2003). To understand the force-generating capacity of the leg, the force "volume" spanned by all combinations of maximum muscle activations was analyzed. The maximum force-generating capacity of the leg was also examined when the moments at the toe were constrained to be zero. Anatomically, the toe can not transmit high moment amounts at the ground because it has small dimensions. Lastly, the effect of changing hindlimb posture on force generation was investigated.

4.1 Single Muscle Forces

For verification of the model compared to both the Burkholder model and experiments, and for understanding individual muscle contributions to end point forces, the end-effector system of each muscle was calculated separately. Since we use the Jacobian method, the system is linear. Therefore, actions of each muscle are simply summed to produce a given end point force system using this useful method.

4.1.1 Methods

First, the effect of each muscle force is transmitted to the toe of the hindlimb by adopting a single equation that calculates the end point force and moment subject to known values of muscle activations. In each case, one of the 31 muscles was maximally activated; the others had an activation value of zero in the default stance position. The torque at the joint or joints that each muscle spans was calculated using the moment arms obtained from the SIMM model at that posture. The effect of the joint torque/torques was transferred to the end point using the inverse transpose Jacobian matrix. For each muscle an end point force system composed of forces in the x, y, and z directions, and moments in the x, y, and z directions (F_x, Fy, Fz, Mx, My, Mz) were computed. The ground reaction force vectors on the cat hindlimb are equal and opposite of the force and moment vectors generated by the hindlimb at the end point.

We also investigated how the individual muscle forces at the end point change for different postures. The "force constraint strategy" is weaker for small stance distances and stronger for large stance distances. To understand how each muscle affects this, the whole leg was moved so the toe was more anterior or more posterior then the default position. All retracted and protracted stance distances and joint angles were taken from the experiments of Macpherson (1994). The same calculation method used for the default posture was utilized for the above postures.

4.1.2 Results

Each muscle generates a distinct force direction at the toe. Although every muscle has a specific end point force, they can be generally categorized as flexors, extensors, adductors, and abductors at each posture of the hindlimb. In Figures 21 through 26 the end point force directions of each muscle are illustrated in the General Coordinate System. Figures show that BFP, EDL, GRAC, PB, PL, PT, PSOAS, PYR, SART, ST, TA have primarily flexor action; ADF, ADL, BFA, FDL, FHL, GMAX, GMED, PEC, QF, RF, SOL, TP, VI produce primarily extensor forces; GRAC, PB, PT are mainly adductors; and FDL, GMAX, GMED, GMIN, PYR, RF, TP can be grouped as abductors (See Table 2 for what muscle abbreviations stand for). Figures 21 and 22 show the directions and magnitudes of the end point forces in the lateral view. The origin corresponds to the toe. Respectively, Figures 23 and 24 are the top view, and 25 and 26 are the posterior view of the directional forces. The components of the end point forces confirmed the existence of non-sagittal forces produced by flexors and extensors (Lawrence, 1993).

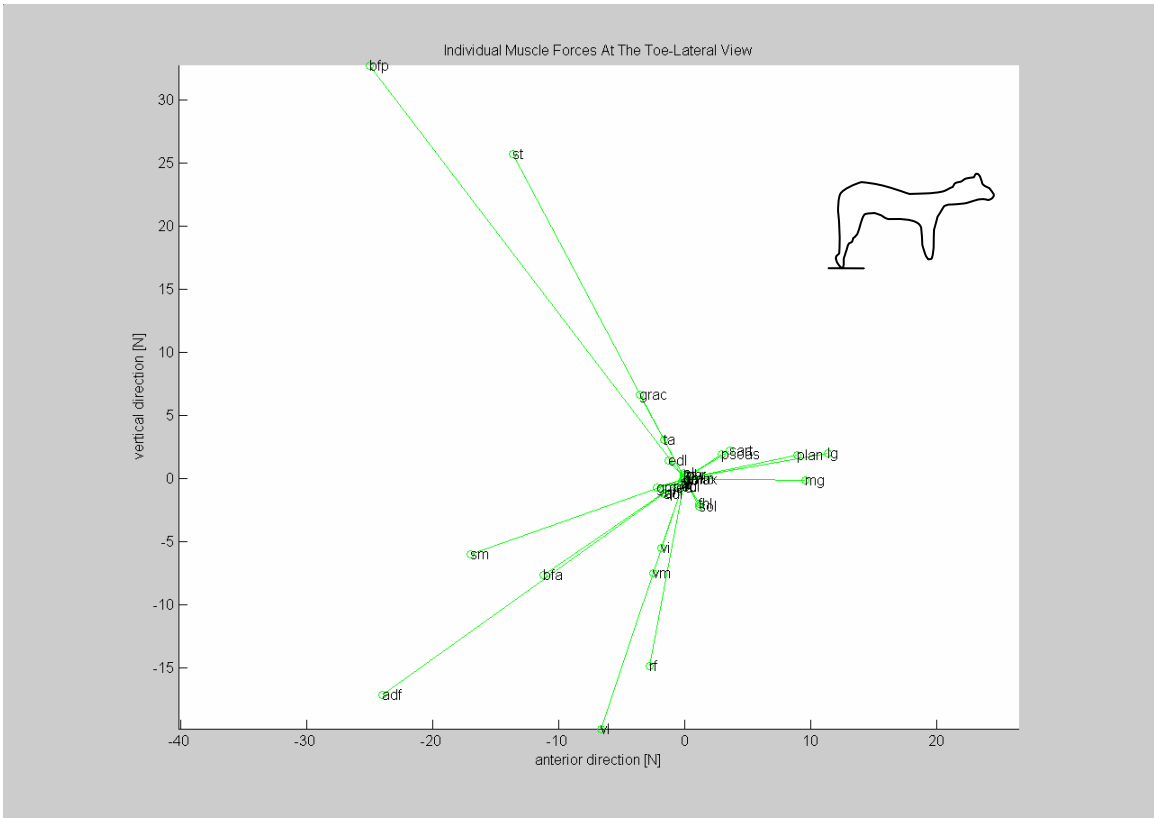

Figure 21: Directions and magnitudes of single muscle end point forces in the lateral view in default posture.

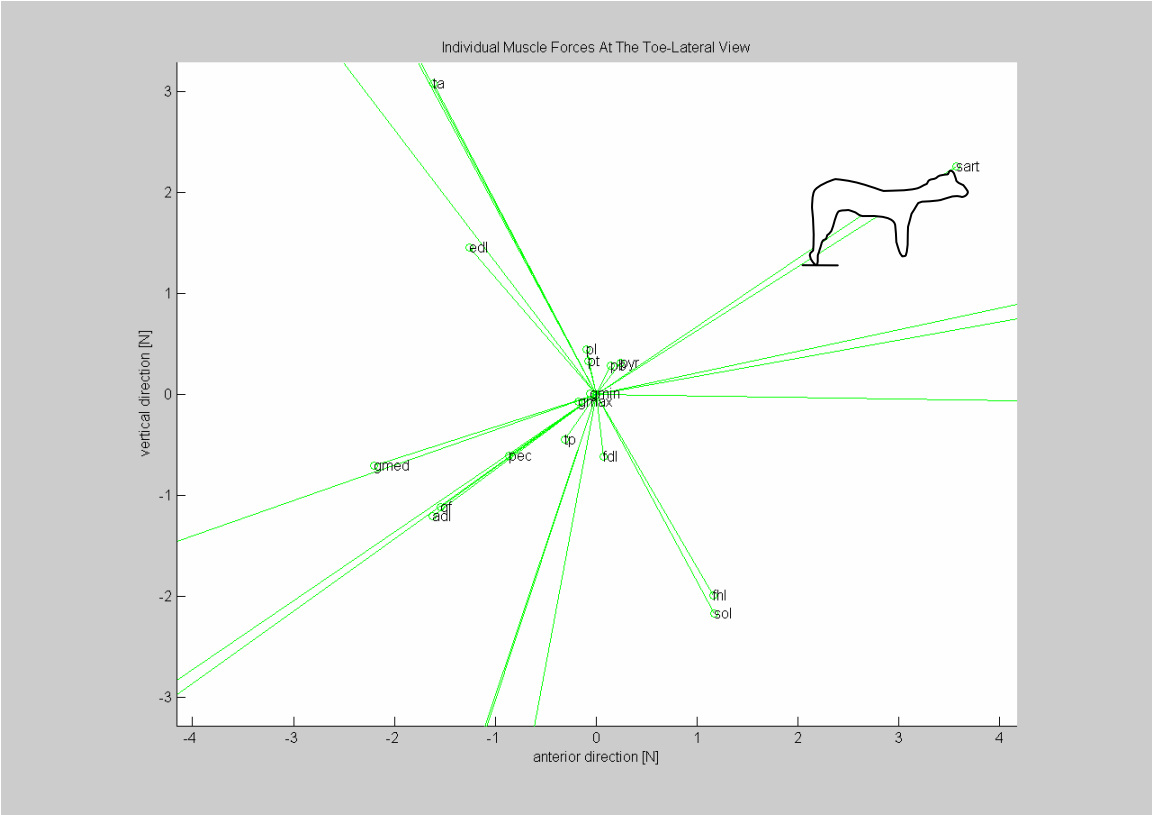

Figure 22: Directions and magnitudes of single muscle end point forces in a closer lateral view in default posture.

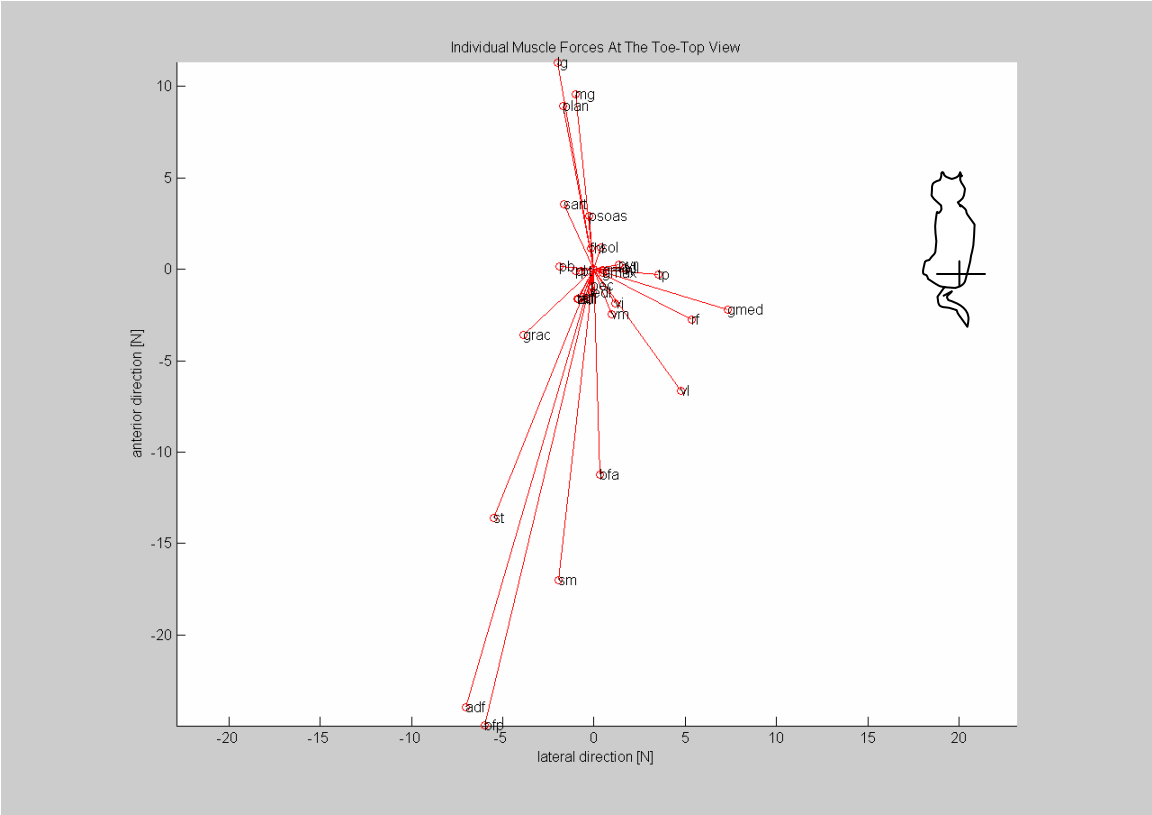

Figure 23: Directions and magnitudes of single muscle end point forces in the top view in default posture.

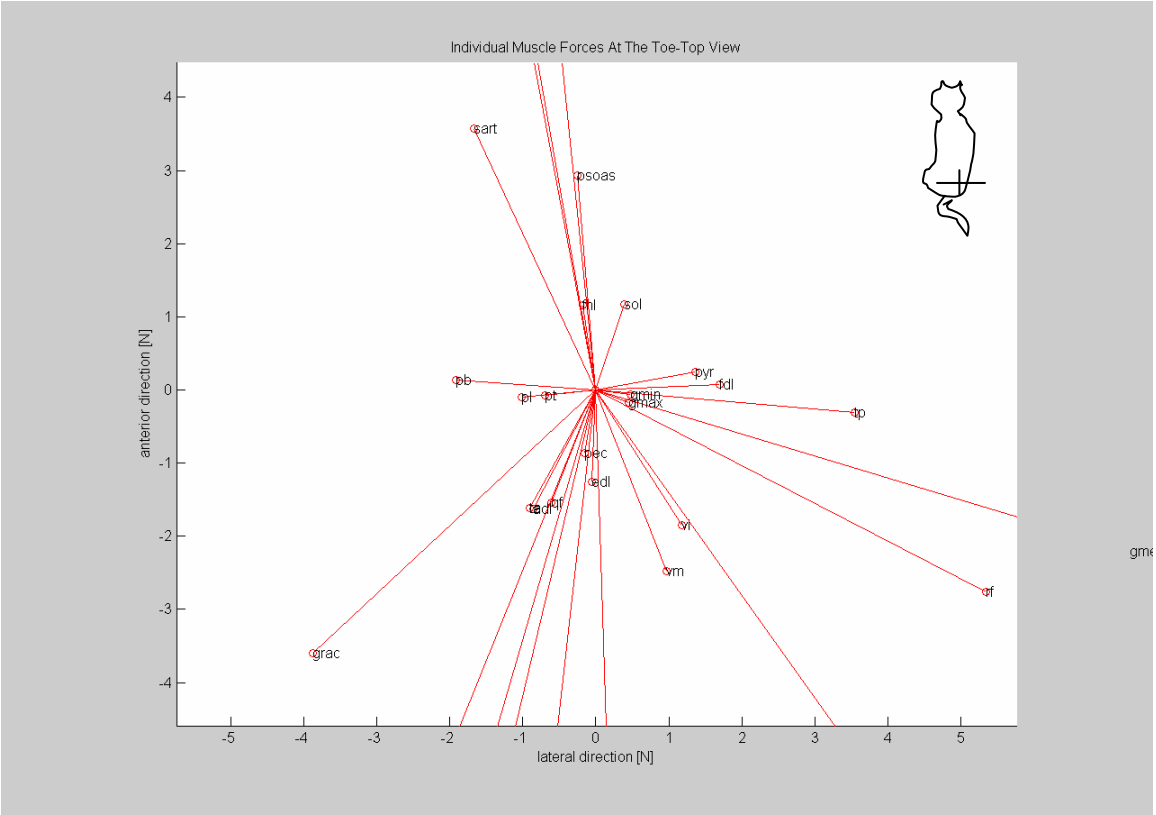

Figure 24: Directions and magnitudes of single muscle end point forces in closer top view in default posture.

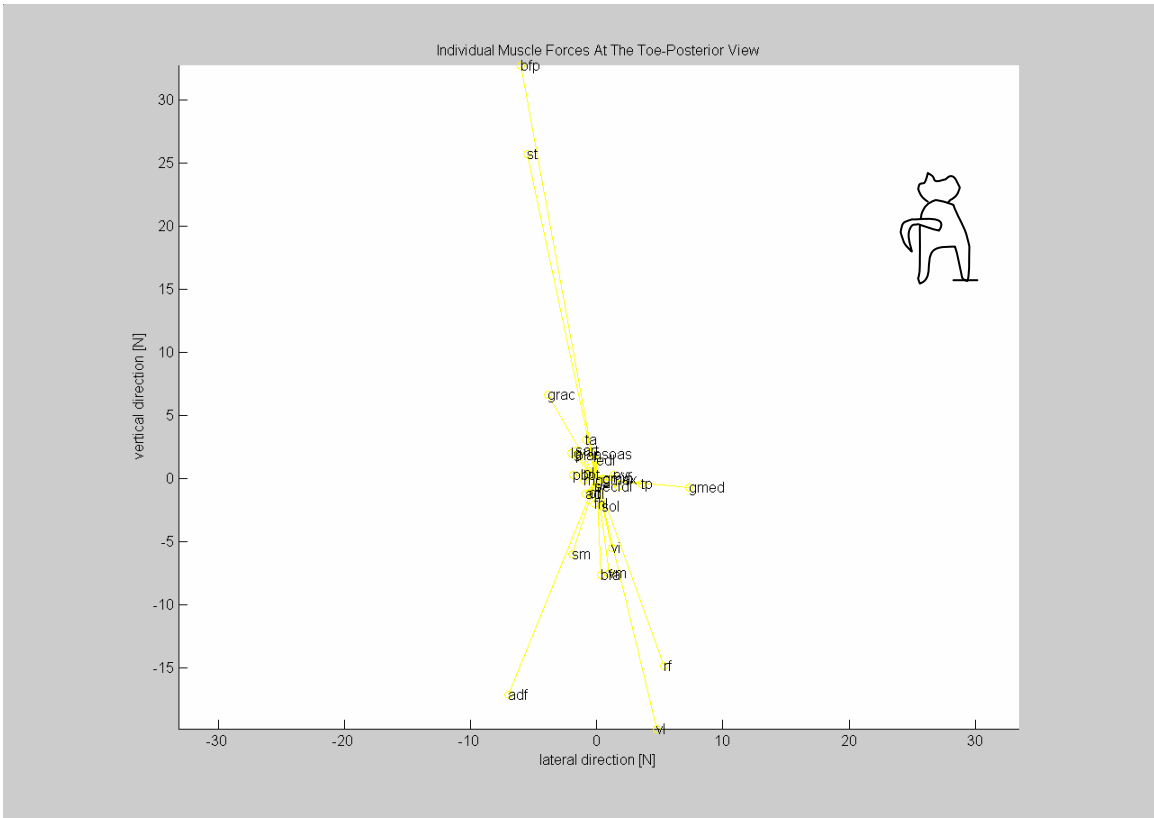

Figure 25: Directions and magnitudes of single muscle end point forces in the posterior view in default posture.

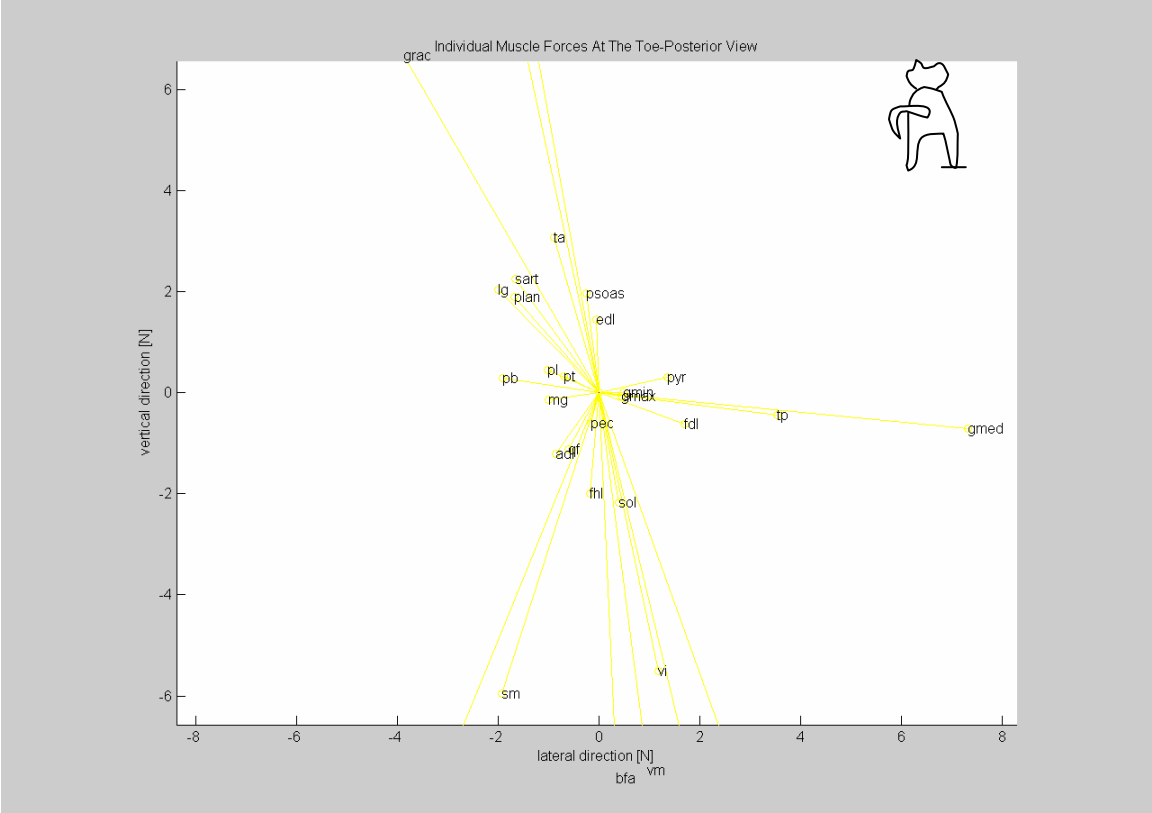

Figure 26: Directions and magnitudes of single muscle end point forces in a closer posterior view in default posture.

Single muscle end point forces were calculated for different postures of the hindlimb. The posture of the hindlimb affected the single muscle end point forces only slightly (See Figures 27-30). The first sub-plot in Figures 27 – 30 shows orientations of the hindlimb segments from the toe located at the origin to the hip.

In the protracted posture (1) (Figure 27) where the stance distance was 18 cm, muscles BF, ST, GRAC's end point forces changed the most. The protracted posture (2) (Figure 28) and preferred posture (Figure 29) had similar muscle end point forces. The retracted posture had the most similar values to the default posture's muscle end point forces. For example, the BF direction has almost no medial-lateral component in the protracted position (1), but a larger medial-lateral component as it goes to the retracted position.

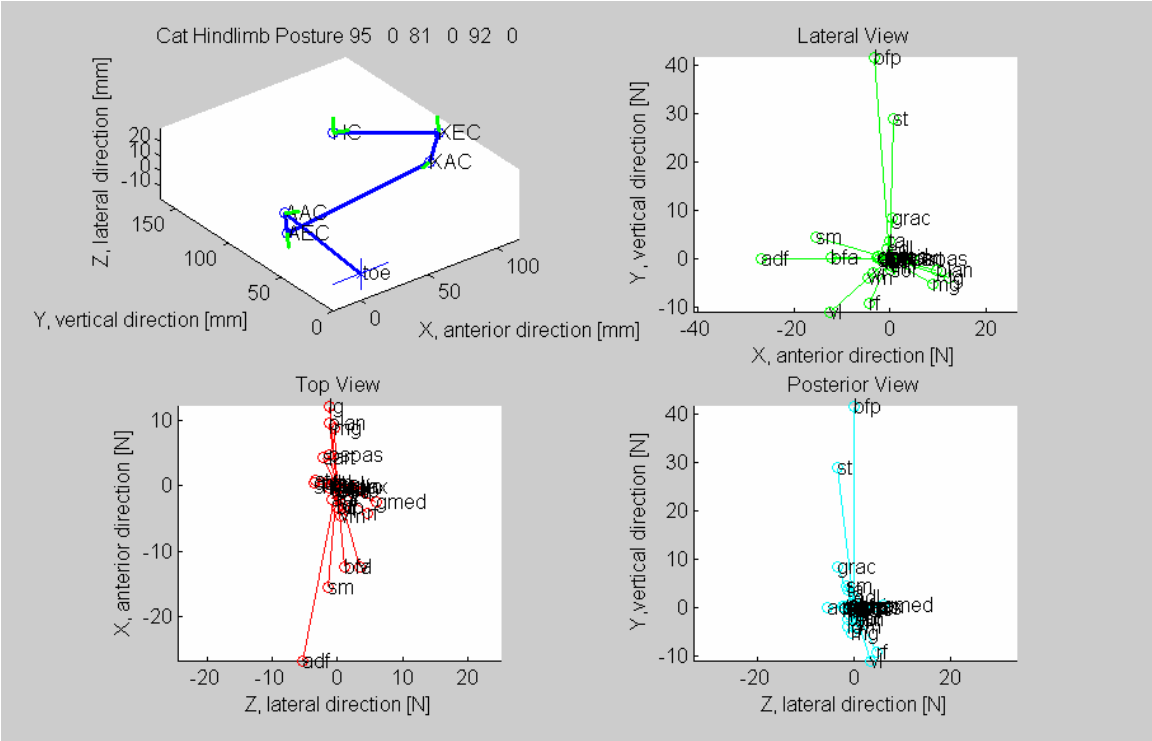

Figure 27: Single muscle end point forces in the protracted posture (1) of the hindlimb (18 cm between the forelimbs and the hindlimbs).

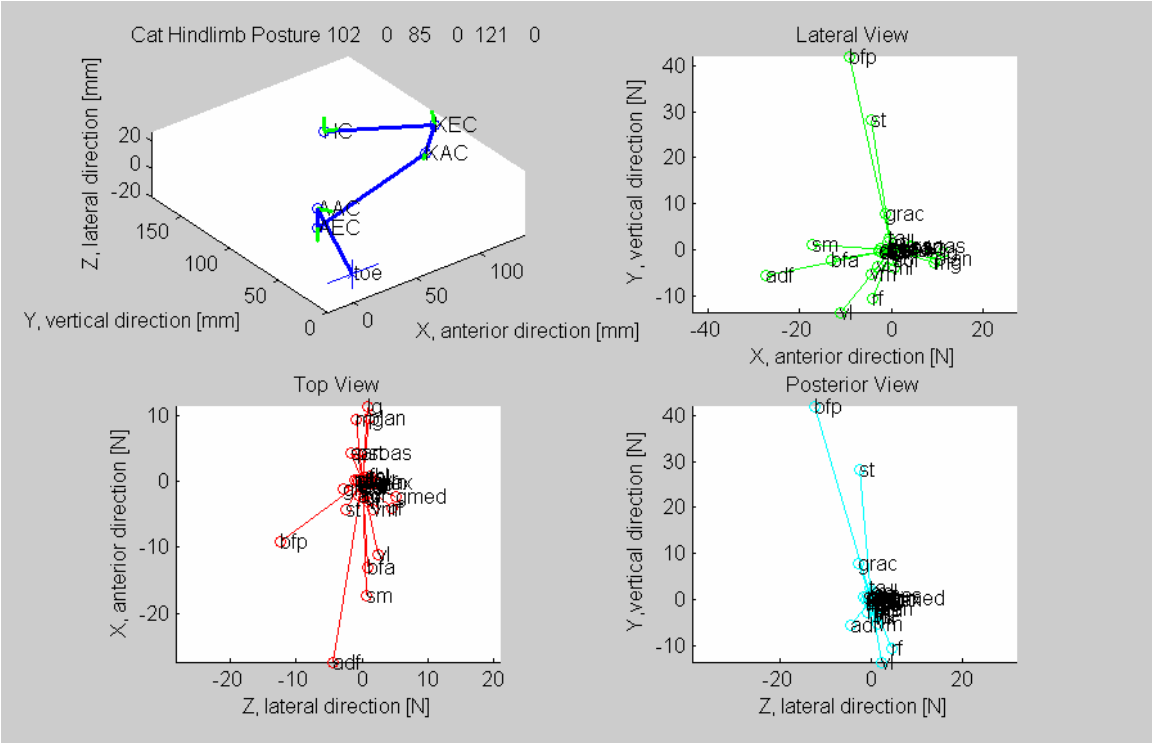

Figure 28: Single muscle end point forces in the protracted posture (2) of the hindlimb (24 cm between the forelimbs and the hindlimbs).

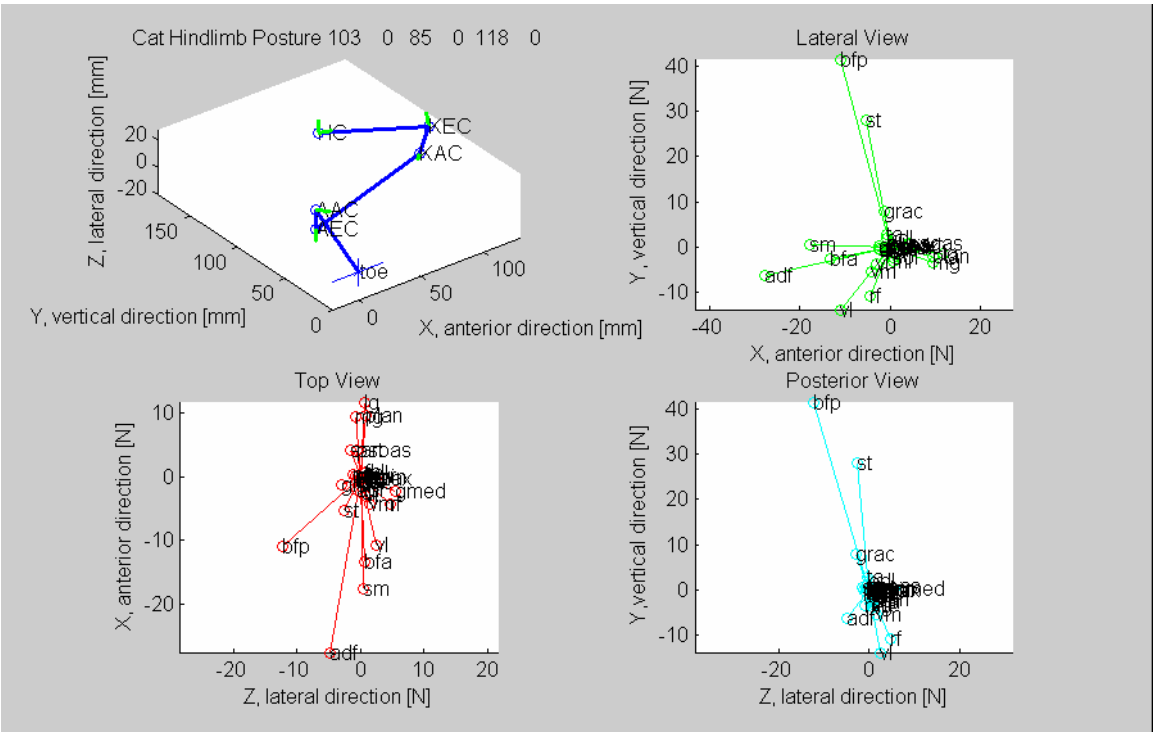

Figure 29: Single muscle end point forces in the preferred posture of the hindlimb (28 cm between the forelimbs and the hindlimbs).

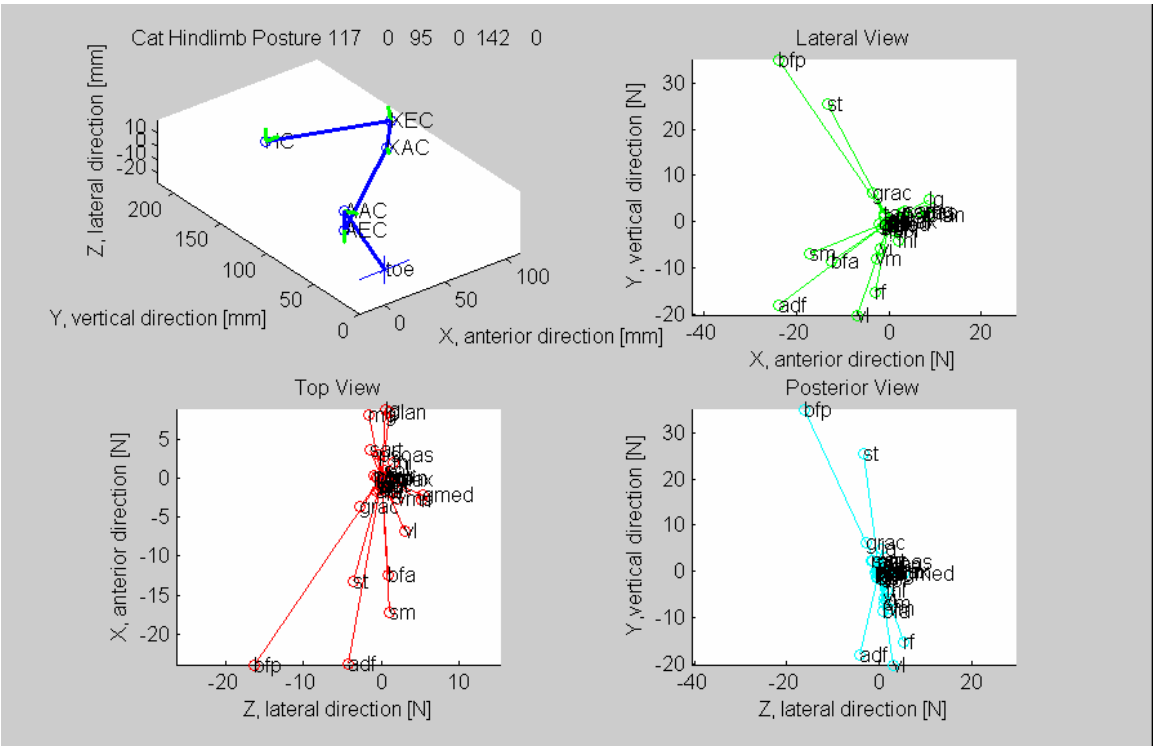

Figure 30: Single muscle end point forces in the retracted posture of the hindlimb (39 cm between the forelimbs and the hindlimbs).

The concentration of this study is on the end point forces of the cat hindlimb. Due to the dimensions of the toe, the cat hindlimb can not even apply small moments (See Section 4.3.1). The magnitude of the end point moments for each muscle of the model varies between 0.01 Newton-meters and 2 Newton-meters. Muscles having the end point moments close to the upper limit of this large range should be recruited carefully for realistic results (See Section 4.3.1 for realistic end point moment values). The moments corresponding to each muscle at the toe were not analyzed. Also, the experiments and the studies in the literature do not report end point moment values.

4.1.3 Discussion

We compared endpoint force results from experimental and modeling studies with our model's results. Some of the end point forces generated by the individual muscles were not consistent with our findings.

Generally, muscles having higher end point forces span the proximal joints, produce larger maximum isometric forces, and have larger moment arms. The muscle BFP exerted the maximum amount of end point force. The primary reason was it has the highest isometric force amount (170 Newtons). Other properties such as large moment arms about proximal joints hip and knee contributed for the transformation of its high isometric force to the ground. Like BFP, PSOAS has a large isometric force and crosses the hip. However, PSOAS' moment arm is not big enough to exert as large end point force as other muscles (i.e. hip flexion-extension moment arm of PSOAS is 2.72mm and BFP is 30.64mm, and hip adduction-abduction moment arms of PSOAS and BFP are

0.12 and 3.49mm, respectively). GRAC's isometric muscle force is small. Since GRAC spans proximal joints with significant moment arms (around 30mm both around hip and knee joints), it created a noteworthy end point force. Except for LG, MG, and PLAN, ankle muscles did not generate significant end point forces. Although FHL can produce as much isometric force as LG, FHL's moment arms about the ankle joint are small.

The first study we compared to our model was on experiments in acute cat preparations, (Murinas 2003) where intermuscular stimulations were performed. In their experiments, end point non-sagittal force directions of muscles were measured and plotted on tuning curves. The transmitted forces of the BFP, GMED, GRAC, SART, and ST muscles have the same direction as our results. On the contrary, LG, MG, VM and VL all had opposite directions.

A possible reason why the data from Murinas experiments deviate from ours is the posture of the cat hindlimb was not necessarily the same between the two studies.

The second study under comparison is the Burkholder model. To understand if the deviations are the outcome of the default posture of the hindlimb, end point forces of the Burkholder model were compared with our model and tabulated below in Table 7. The Burkholder model has the same postural and muscle connection data as our model; however, some of the end point forces were still different.

Differences in the kinematic parameters affecting the functional groupings of the muscles may be a possible reason why the results were not consistent with ours. As an example for the kinematic parameters, adduction-abduction moment arms play an important role in applying medial and lateral end point forces (Young et al., 1992). The magnitude and sign of these moment arms change as the joint angle changes. Therefore, the moment arm of a muscle compared with corresponding moment arms of other models should serve for similar functions such as a flexor, an adductor, etc. As mentioned in the moment arm validation section of 2.4.2, the abductor-adductor moment arms of the Burkholder model differed from ours. However, all knee and ankle flexion-extension moment arms were consistent; the end point forces of knee and ankle flexor-extensor muscles were in different directions between our model and Burkholder's. Further, although there were differences in flexor-extensor moment arms, the sign of the moment arms did not change, and therefore a difference in direction of the endpoint force was not expected.

Our constraint on the hip internal-external rotation could be invalid. There are other possible reasons for the differences. First, the results from Burkholder model were computed by running forward simulations of individual muscle activations while the joints were stiffened by spring elements. However, the muscles were activated only a small amount to minimize the movements of the leg. Second, the toe has an articulated morphology in two modeling and experimental studies unlike the point toe in our model. The most important of all, the femur was fixed in Burkholder model as opposed to our

pelvis fixed model. Two degrees of freedom (hip flexion and hip adduction) were not considered in the Burkholder model.

Table 7: End point force comparison with Burkholder model.

	Burkholder	**Jacobian**
EDL, TA	Lift & anterior	Lift & posterior
BF, GRAC, ST	Lift & posterior	Lift & posterior
RF, VI, VL, VM	Support weight & anterior	Support weight & posterior
FHL, SOL, MG, LG, PLAN	Support weight & posterior	Support weight & anterior (LG, PLAN lift)
PB, PL	Lateral force	Medial force
FDL, TP, PT	Medial Force	Lateral force (PT medial)

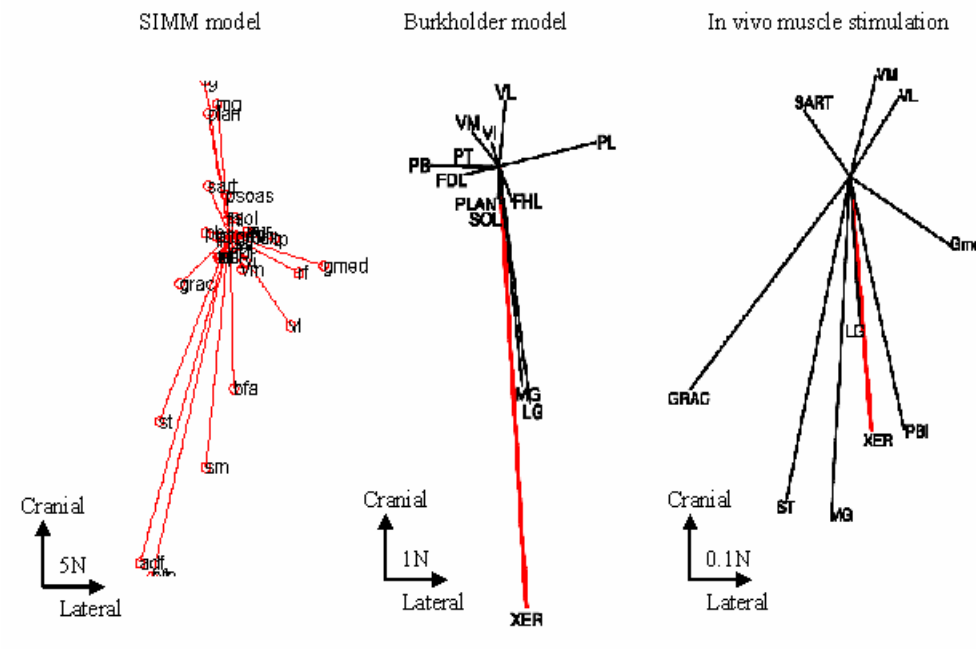

Figure 31: Transformed single muscle forces to the end point in the top views of the SIMM model, Burkholder model and Murinas in vivo muscle stimulations.

Overall results show that knee and ankle muscles of our model generate forces in opposite directions to the Burkholder and Murinas' corresponding end point forces of knee and ankle muscles (See Figure 31). We examined if the factor affecting the directional forces inversely, arise from moment arms or the static method employed. This ambiguity led to further investigation of the Jacobian matrix. Twelve idealized mono-articular muscles having unity moment arms and spanning all six mechanical joints were created. Each of them represented a joint function such as: hip flexion, extension, adduction, abduction; knee extension, etc (twelve in total, representing six mechanical joints forced in two opposite directions). Thus, the idealized muscles were pure joint torques. The Jacobian method pointed out the end point forces of the functional muscle groupings at the joint level as follows (See Figure 32):

Hip flexors in anterior and negative gravity direction;

Hip adductors in medial direction;

Knee extensors in posterior, gravity, and slightly lateral direction;

Knee adductors in lateral and gravity direction;

Ankle extensors in anterior and gravity direction;

And ankle adductors in lateral direction.

End point forces of the functional muscle groupings were different than the experimental single muscle results. For example, ankle extensors were in the anterior and gravity directions in the Jacobian method, as opposed to the posterior and gravity directions of the ankle extensor muscles in experiments. The Jacobian matrix can not be incorrect because it was independently verified using two methods.

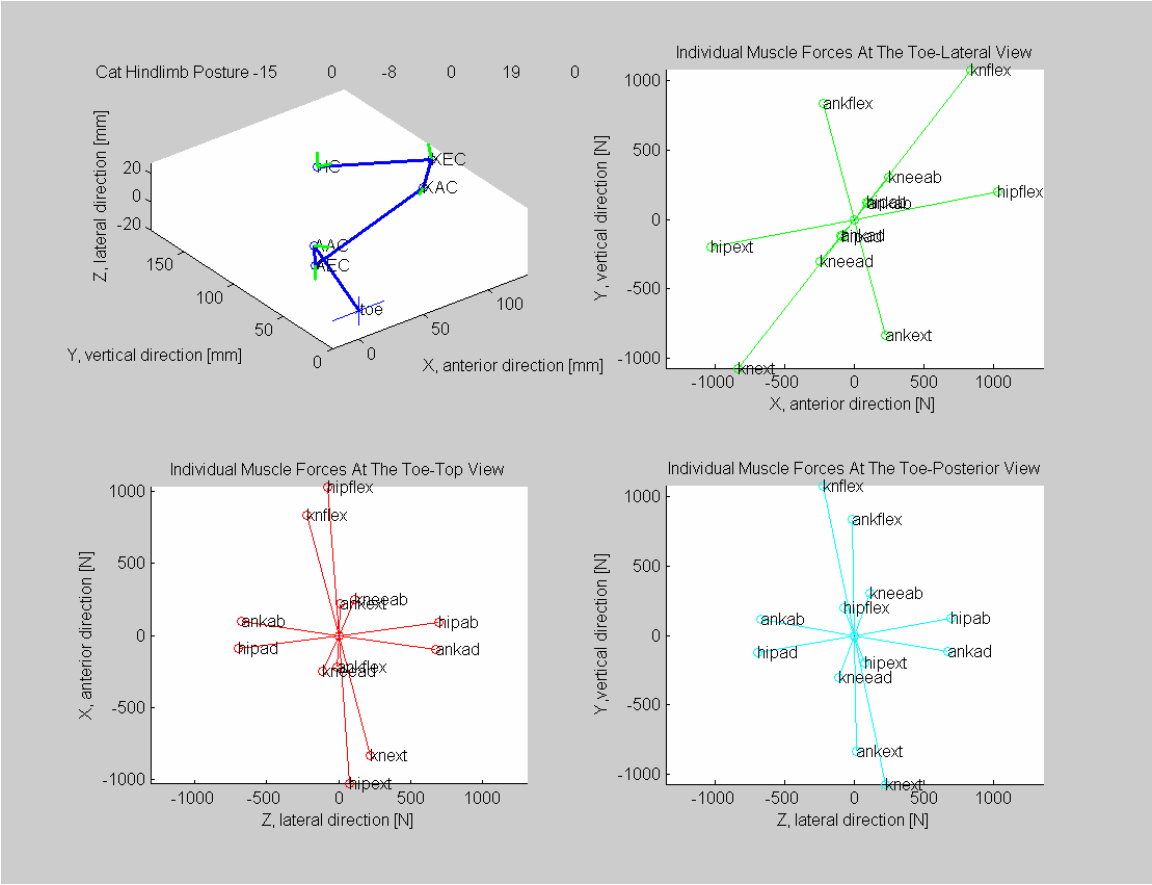

Figure 32: Ideal muscle end point force directions corresponding to pure joint torques in the default posture.

Therefore, the static-kinematic method employed is an essential issue in the determination of the end point forces more than anatomical attachment points of the muscles, moment arms and the joint parameters. Also, posture contributes to the calculation of muscle moment arms and end point forces. For example, the hip joint angle of the retracted posture (stance distance 39) is similar to the default posture hip joint angle. Hip moment arms are dominant compared to knee and ankle moment arms. Thus, the end point forces of the strong muscles BFP, GRAC, and ST were consistent within the default and retracted postures. The deviation of the muscle moment arms for the protracted and preferred postures varied within 2mm. Also, these moment arms differed from the default posture muscle moment arms by approximately 2mm. In some cases the moment arms differed by 5mm. Joint parameters (i.e. joint rotation vector and joint center position in the Global Coordinate System) depend on the posture. However, others have successfully used this static method to obtain results similar to experimental values (Valero-Cuevas, 1998).

4.2 Feasible Set of Forces

We next examined which directions and what magnitudes of end point forces the leg can produce as a consequence of multiple muscles. Different combinations of maximally activated muscles in the cat hindlimb were analyzed to visualize the volume constructed by all attainable end point force systems. In a set of 31 cat hindlimb muscles, the number of combinations of maximally activated muscles (bang-bang solution set) is $2^{31} = 2.15e^{9}$. To decrease the computation time created by this huge set of possible muscle coordination patterns, some of the muscles were omitted. In the first part, calculations

were done selecting 10, 12 or 13 muscles. In the second part, muscles were lumped according to their moment arms and maximum force amounts to form 12 muscle groups.

4.2.1 Individual Muscles

By choosing different muscles, the end point force range was constructed. For every case 10 to 13 muscles were selected. In the selection, muscles spanning different joints and rotating the joints in different directions (e.g. flexion, adduction) were included. The magnitudes of the maximum muscle forces was also important in the selection. Each muscle has a distinct effect at the toe highlighted by the single muscle forces in section 4.1.

In each case, joint torques created by the activated muscles were calculated by the equation $\boldsymbol{\tau} = \mathbf{RF}_{max}\mathbf{e}$. '**e**' is a column vector, each entry of which corresponds to a muscle activation level (Section 3.3.1). Different combinations of **e** vectors were concatenated to form an activation matrix. The activation matrix was substituted into the joint torque equation and a joint torque matrix was created for each case. Every column of the joint torque matrix corresponds to one activation pattern **e**. The rows are hip flexion, hip adduction, knee extension, knee adduction, ankle extension, and ankle adduction, respectively. Using the Jacobian matrix, the joint torques were mapped to the end point forces similarly as in the single muscle forces in Section 4.1. As a result, every muscle activation pattern (e vector) creates a vector in the bang-bang solution set. Altogether, these solutions produce a feasible solution volume. Lateral, top and posterior views of this volume are shown in Figures 33-35 for some of the cases.

4.2.2 Lumped Muscles

The feasible force region was plotted for lumped muscles (See Figure 36). The same procedure was followed as in the individual muscle cases above except that the maximum force amounts taken from the literature were adjusted according to the muscles that were lumped together. Muscles were grouped according to the similarity of their moment arms. Muscles rotating the joints in the same directions were selected. In each group, a muscle with the largest amount of maximal force was selected as a main muscle. The other muscles were named as secondary muscles.

The force amount of a lumped muscle was formed by combining the force amount of a main muscle with the force amounts of a secondary muscle or muscles within its group. Moment arms of the lumped muscles were equated to the moment arms of the main muscles. In each group, the ratio of the moment arm of a main muscle to the moment arm of the secondary muscle of each mechanical joint was calculated. The largest of the magnitudes of these ratios among the main muscle and the secondary muscle determined the amount to strengthen the main muscle. That is, the maximum force capacity of the main muscle was increased proportional to the inverse of the largest ratio. Thereby, the effect of secondary muscle or muscles was underestimated while lumping with the main muscle. For example, a main muscle GMED (originally 60 Newtons) was combined with secondary muscles GMAX and GMIN to an adjusted maximum force generation capacity of 66.45 Newtons.

4.2.3 Results

Muscles were maximally turned on and off, and the feasible force region was constructed to identify the biomechanical constraints that may determine the hindlimb force strategy against perturbations. The range of forces does indicate some limitations. The force production capability of the hindlimb is dominated by extensor muscles.

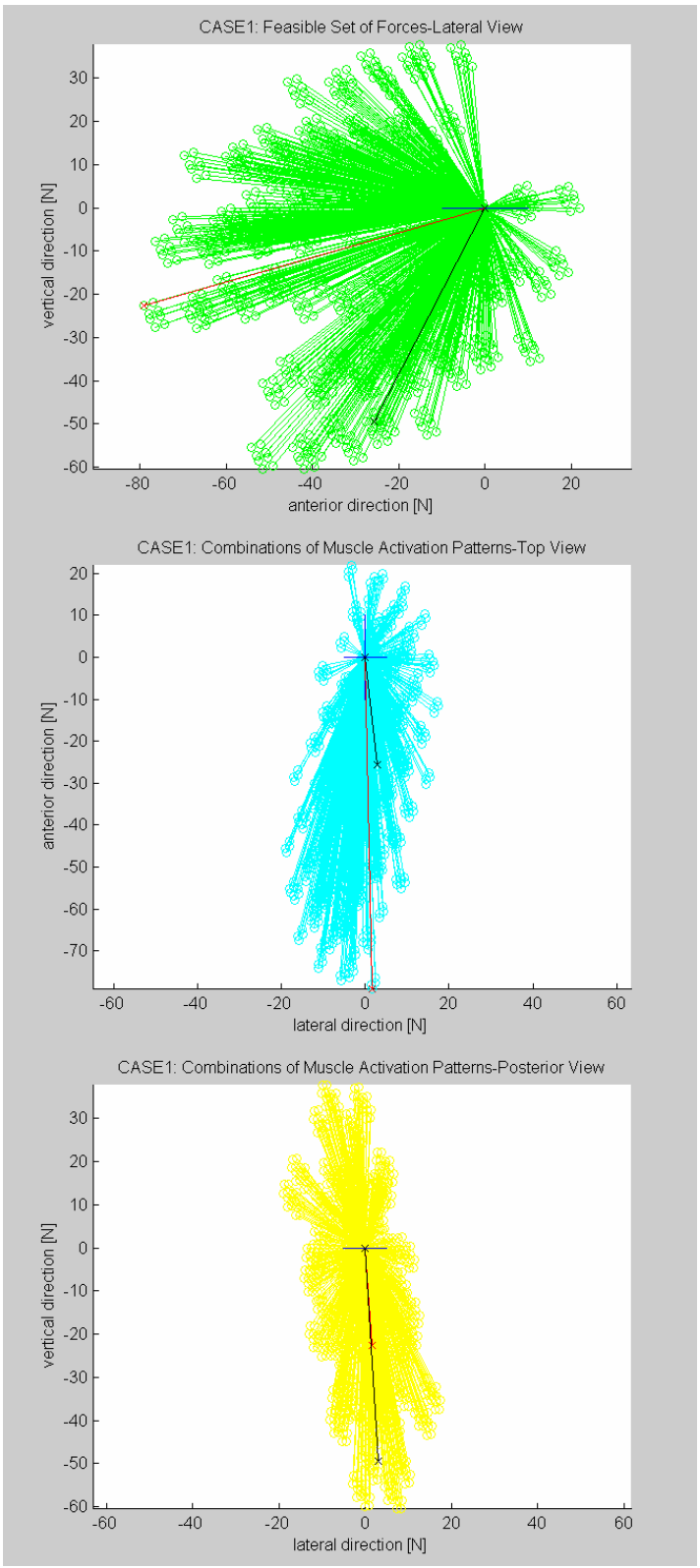

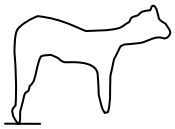

Figure 33: Feasible force set constructed for 10 muscles (adf,bfp,fhl,gmed,lg,mg,rf,sm,ta,vl), and unconstrained (red line) and constrained (black line) optimization results of Section 4.3.

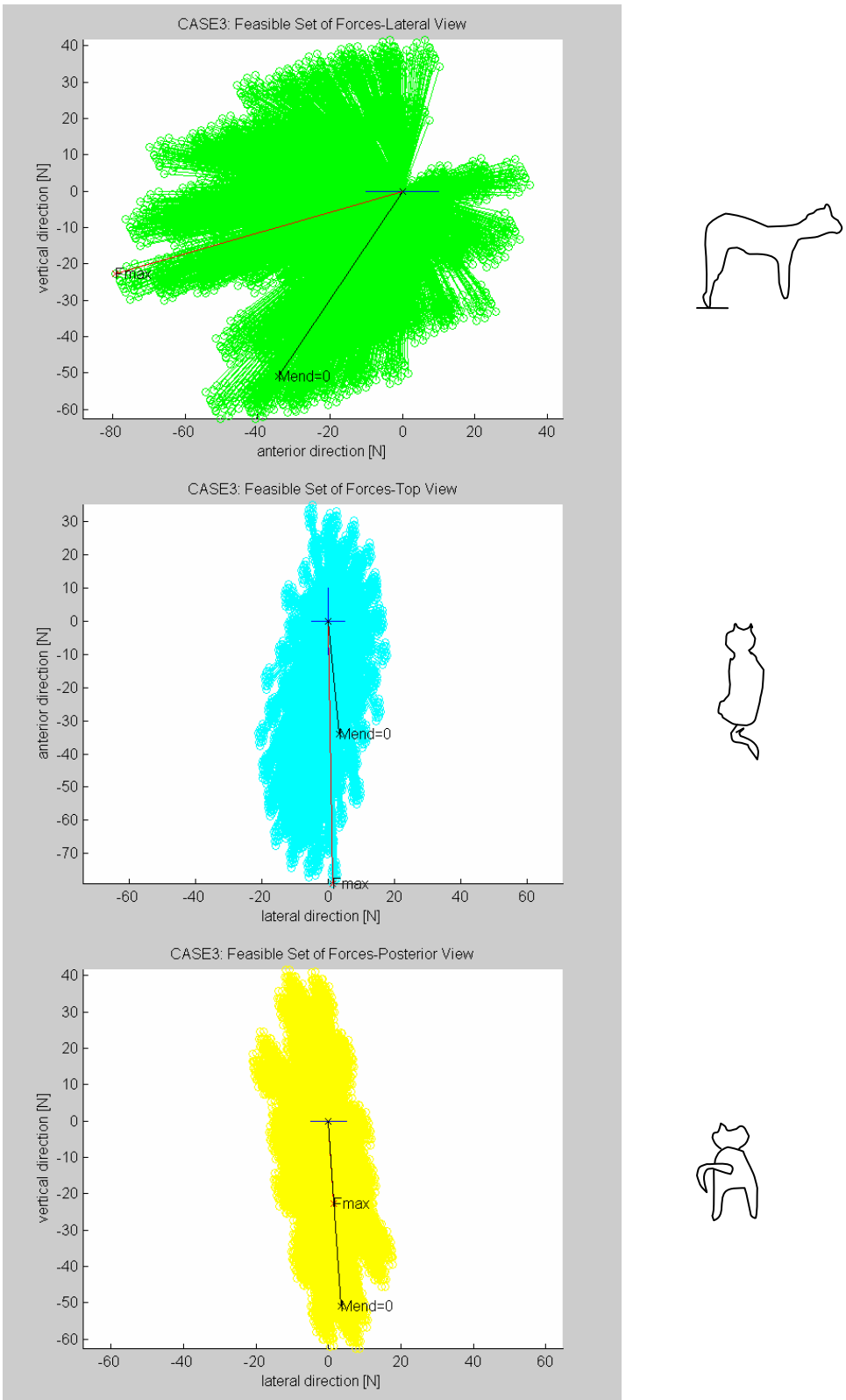

Figure 34: Feasible force set constructed for 13 muscles (adf,bfp,fhl,gmed,lg,mg,plan,psoas,rf,sm,sol,ta,vl), and unconstrained (red line) and constrained (black line) optimization results.

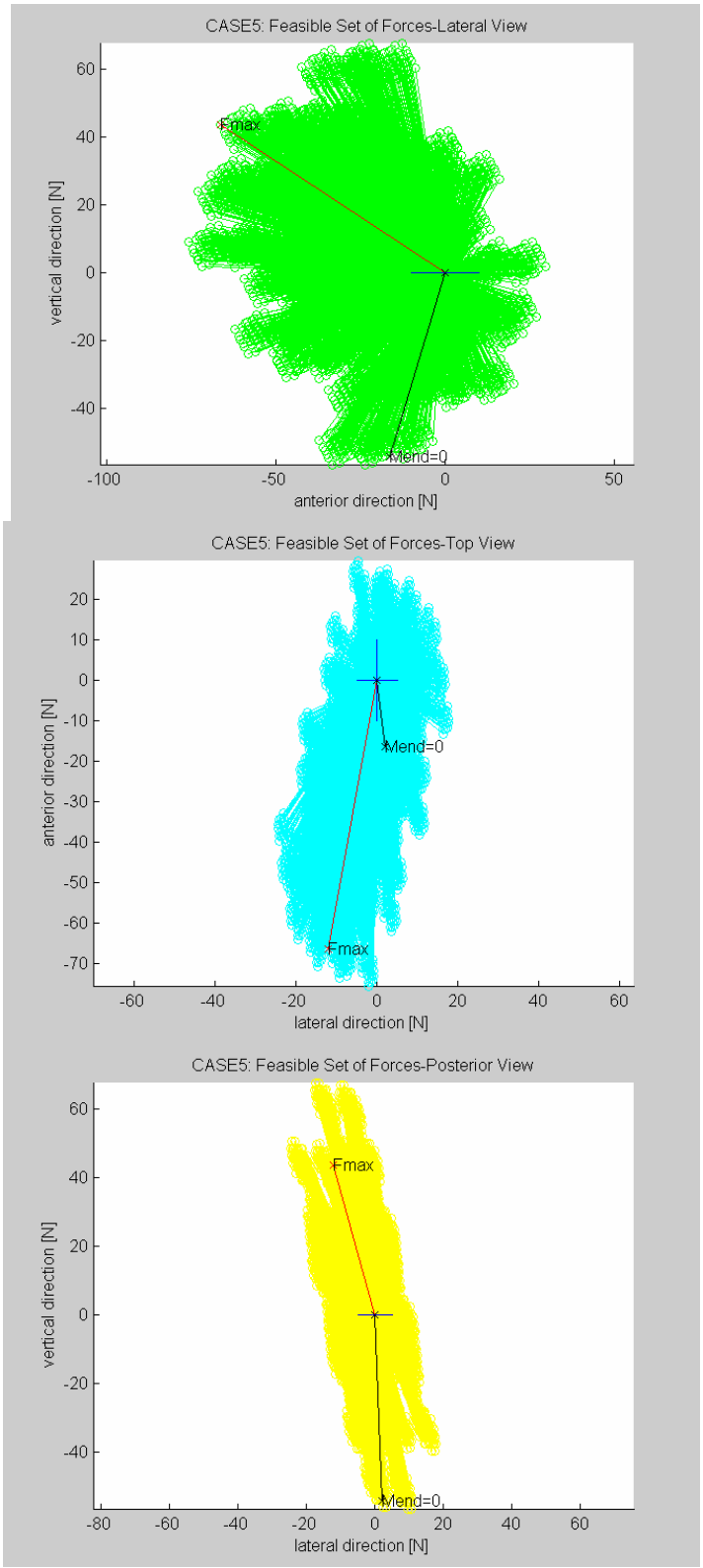

Figure 35: Feasible force set constructed for 13 muscles (adf,bfp,fhl,gmed,lg,mg,psoas,rf,sart,sol,st,ta,vl), and unconstrained (red line) and constrained (black line) optimization results.

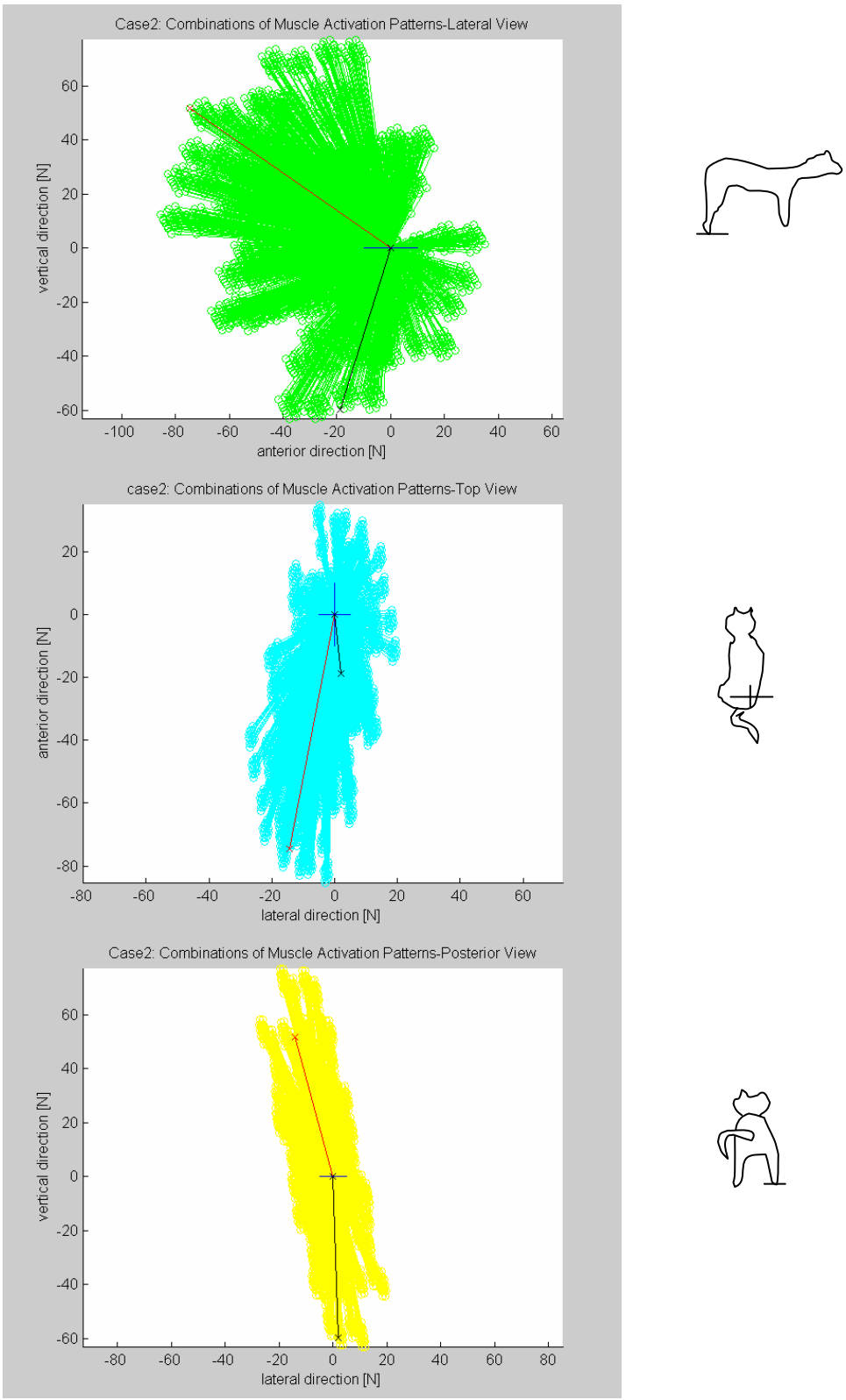

Figure 36: Feasible force set constructed for 12 lumped muscles (adf,bfp,fhl,gmed,lg,mg,psoas,rf,st,sol,ta,vl), and unconstrained (red line) and constrained (black line) optimization results.

The feasible region spanned is roughly a volume similar to three quarters of a cylinder. In Figures 33-36 (Figures 33-35 show some of the single muscle cases and Figure 36 displays the lumped muscle case), and the lateral view of the cat shows the bottom and top areas of the cylinder. The missing quadrant is in the anterior and negative gravity direction. As the number of muscles increased in the feasible force set computations, the range spanned became denser. The volume of the feasible force set did not change much, but some of the unoccupied volume in the figures could be filled out by increasing the muscles recruited. For example, as muscles sartarius (SART) and ilipsioas (PSOAS) were added, they filled the gap of feasible force set towards the anterior direction. Due to computational difficulties, there is a limitation on how many muscles can be included. The available computer memory could be expanded for the feasible force set construction of all the muscles.

For changing stance distances, the volume occupied was more like two ellipsoids next to each other (Figures 37-40). In close stance distances, the ellipsoids were more distinct, whereas in large distances the ellipsoids were more combined. The feasible force set of retracted posture was more like the default posture's volume (See Figure 40).

4.2.4 Discussion

The feasible force region spanned by maximally activated muscles was directed towards the posterior and gravity directions. The extensors push down and back. We can say that extensors play a crucial role in the determination of the force capacity of the leg. In shorter stance distances, flexors were significant, too. Therefore, retracted postures may

have a force application strategy directed in the posterior and gravity directions. This matches experimental data (Macpherson, 1988b). However, there may still be a neural control scheme affecting the force application direction and choices of muscle patterns.

The feasible force set composed from bang-bang muscle activations may not represent the response of the leg to perturbations. Specifically, end point moments produced by maximally activated muscles were unrealistic and a constraint was added to the algorithm. This aspect was further discussed in Section 4.3.

If we wanted to demonstrate the feasible force set region when muscles are sub-maximally activated, it would require long computation times or a suitable software. All possible combinations of the muscle activations (non-bang bang solution sets) give a 31 dimensional muscle activation unit hypercube ($0 \leq e_i \leq 1$, i: muscles). A linear mapping of the 31 dimensional unit hypercube to the end point force system through the Jacobian method (constant $\mathbf{J}^{-\mathbf{T}}\mathbf{R}\mathbf{F}_{\mathbf{max}}$ term) forms a three dimensional convex polyhedron. The polyhedron is the biomechanically feasible force solution set. Thus, a demonstration of the non-bang bang solution set requires more computation time and suitable software programs.

4.3 Maximum Force Generation

The aim of this part of the study was to demonstrate the effect of an achievable moment on the maximum force and muscle activation pattern. An optimization algorithm was performed to maximize the force generation at the end effector without any constraints or

placing constraints on the end point moment. Independent of the muscles recruited in each case, the constrained version gave consistent solutions with sub-maximal muscle patterns. On the other hand, the unconstrained version gave different solutions in different cases with maximal muscle activations.

4.3.1 Unconstrained End Point Force System

Subject to a cost function of generating the maximum magnitude of the end point force in any direction, a biomechanically feasible unique muscle activation pattern **e** was found. The end point moments in the x, y and z directions which are the last three components of the end point force vector, were not constrained. The 'fmincon' function of MATLAB (MathWorks, Inc.) was utilized to maximize the end point force magnitude. The function does a gradient search by changing muscle activation values (e_i) between zero and one. The algorithm was performed for the individual muscles and lumped muscles cases in section of 4.2, in each of which the muscles recruited changes slightly. The endpoint force vectors were plotted on the feasible force set figures to check if they were inside the feasible region (red vectors in Figures 33-36).

The magnitude of the end point moments in each case had an approximate value between four to seven Newton-meters. The magnitude of the maximum end point forces was around 80 Newtons. Force-moment relationship requires a minimum length of 0.05m (=4[Nm]/80[N]) between the center of pressure of the contact area and the end point of the foot in order for the moment to be supported when an 80 N endpoint force is exerted.

Since the toe of the cat is approximately 0.01m, it is impossible for a cat to apply those moments at the ground.

4.3.2 Constrained End Point Force System

The end point moment was constrained for maintaining static posture and obtaining more realistic results. The end point moments were equated to zero in the optimization algorithm. The resultant force vectors were plotted in the feasible force set region and are shown in Figures 33-36 as black lines. Therefore, the assumption of the toe as a point contact was satisfied.

The constrained maximum force value is on the surface of the three dimensional force polyhedron explained in Section 4.2.4. The polyhedron should be constrained for zero end point moments while mapping the unit hypercube through the Jacobian matrix. Every vector ending at a point on the surface of the polyhedron corresponds to the maximum force applied by the toe at the direction vector points. The longest vector among these is the maximum end point force that is biomechanically producible.

4.3.3 Results

The unconstrained end point force system varied among cases, whereas the constrained end point moments were consistent and resulted in solutions with sub-maximally activated muscles. The orders of magnitude of the forces were consistent with the literature values. The end point forces changed from 50 to 100 Newtons considering

constrained and unconstrained cases. Experiments on maximum height jumping by cats shows approximately 100 Newtons can be generated per hindlimb at most (Zajac et al, 1981).

The results of the unconstrained optimization algorithm show that, biomechanically, the magnitude and direction of the maximum possible end point force vector were sensitive to the muscles involved in the algorithm. Therefore, the force vector changed from case to case. In the first case where only 10 muscles were employed, the direction of the maximum end point force was generated in the posterior and downward direction. Inclusion of ST and combining it with the muscles SM and GRAC in the second case shifted the force vector to flexion of the leg, excessively. The third case where 13 muscles were recruited, gave numerically same results as the first case. In other cases, force direction changed depending on the muscles recruited. Overall, the force vector was in posterior direction, and medial-lateral component of the force was negligible. All of the solutions were elements of the feasible set of bang-bang solutions.

In contrast, in the constrained force results, end point force vectors were consistent across different cases and required non bang-bang solutions. All constrained maximum forces were directed towards the gravity and posterior direction (enforcing hindlimb extensors). Although muscle activation patterns were non bang-bang solutions, they were within the bang-bang feasible force region. For example, in case 4, the muscles BFP, GMED, and LG had activation levels of less than one.

Similar results were obtained for different stance distances (Figures 37-40), except for the direction of constrained end point force for one of the cases was in negative gravity direction.

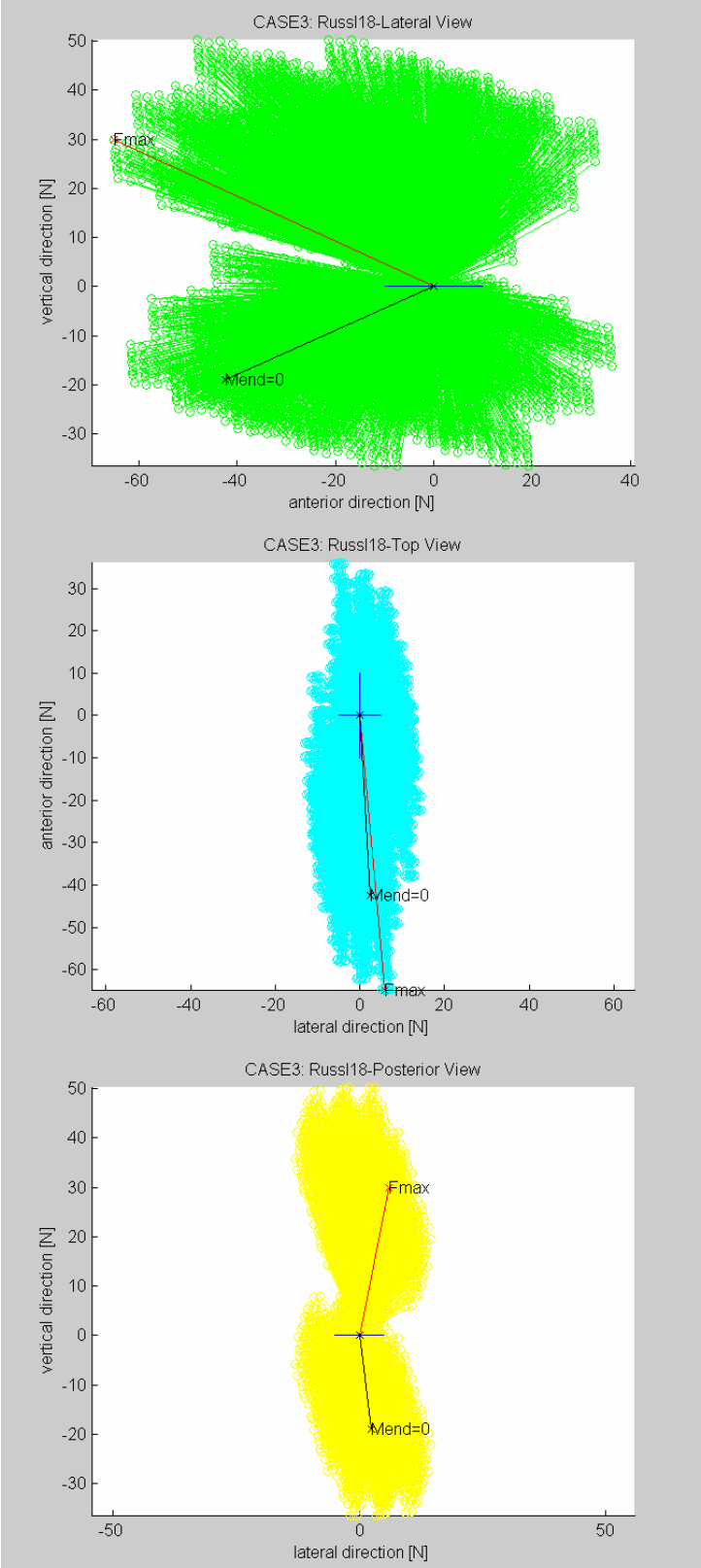

Figure 37: Feasible force set constructed for protracted posture (1), and unconstrained and constrained optimization results.

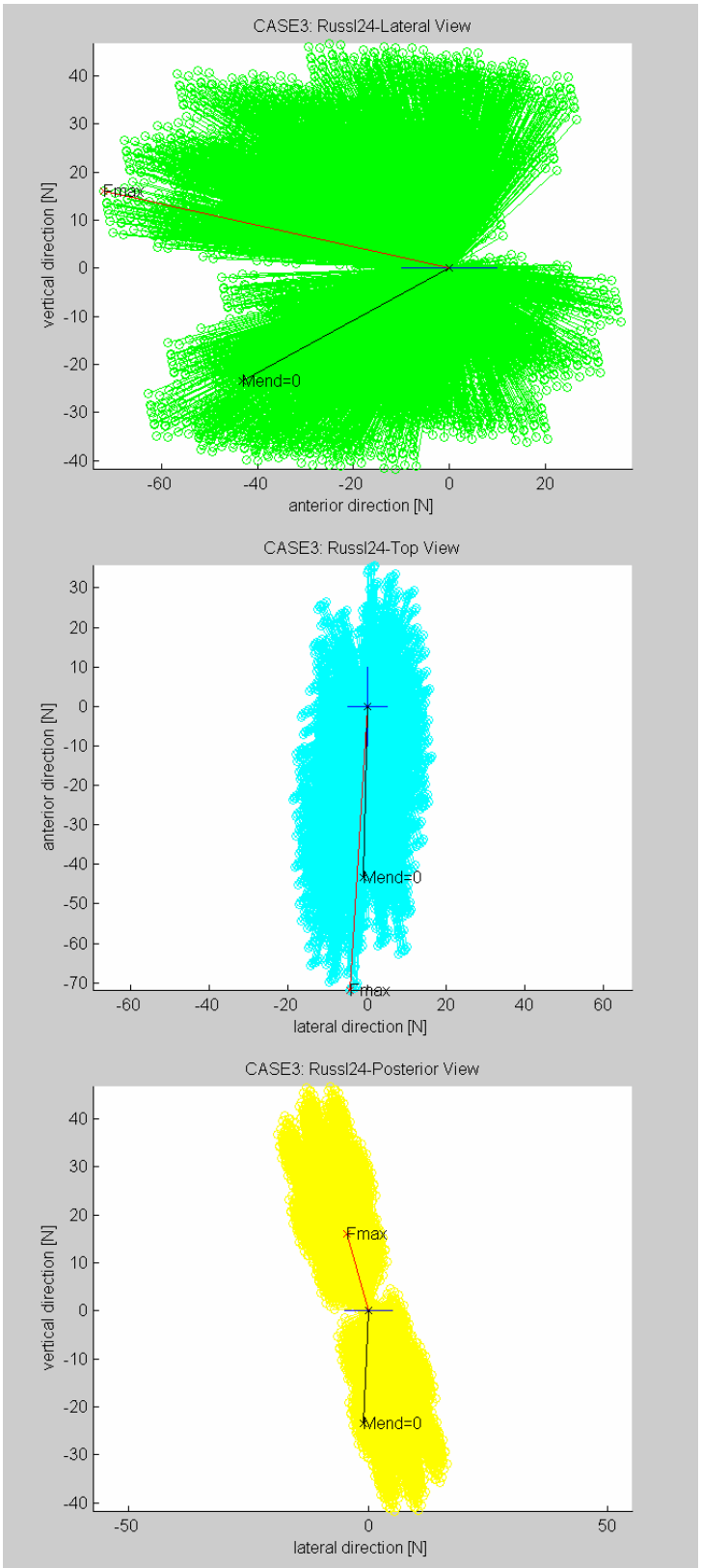

Figure 38: Feasible force set constructed for protracted posture (2), and unconstrained and constrained optimization results.

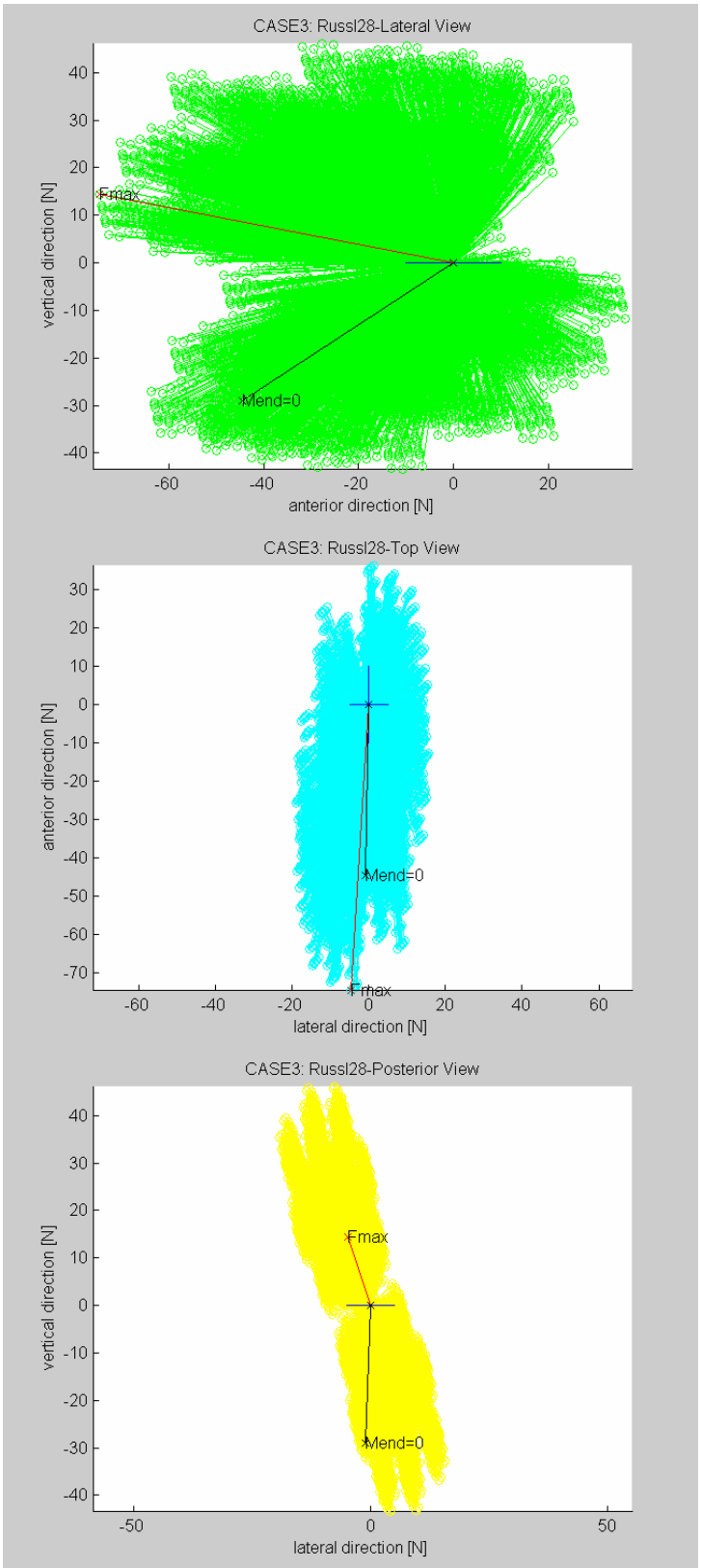

Figure 39: Feasible force set constructed for preferred posture, and unconstrained and constrained optimization results.

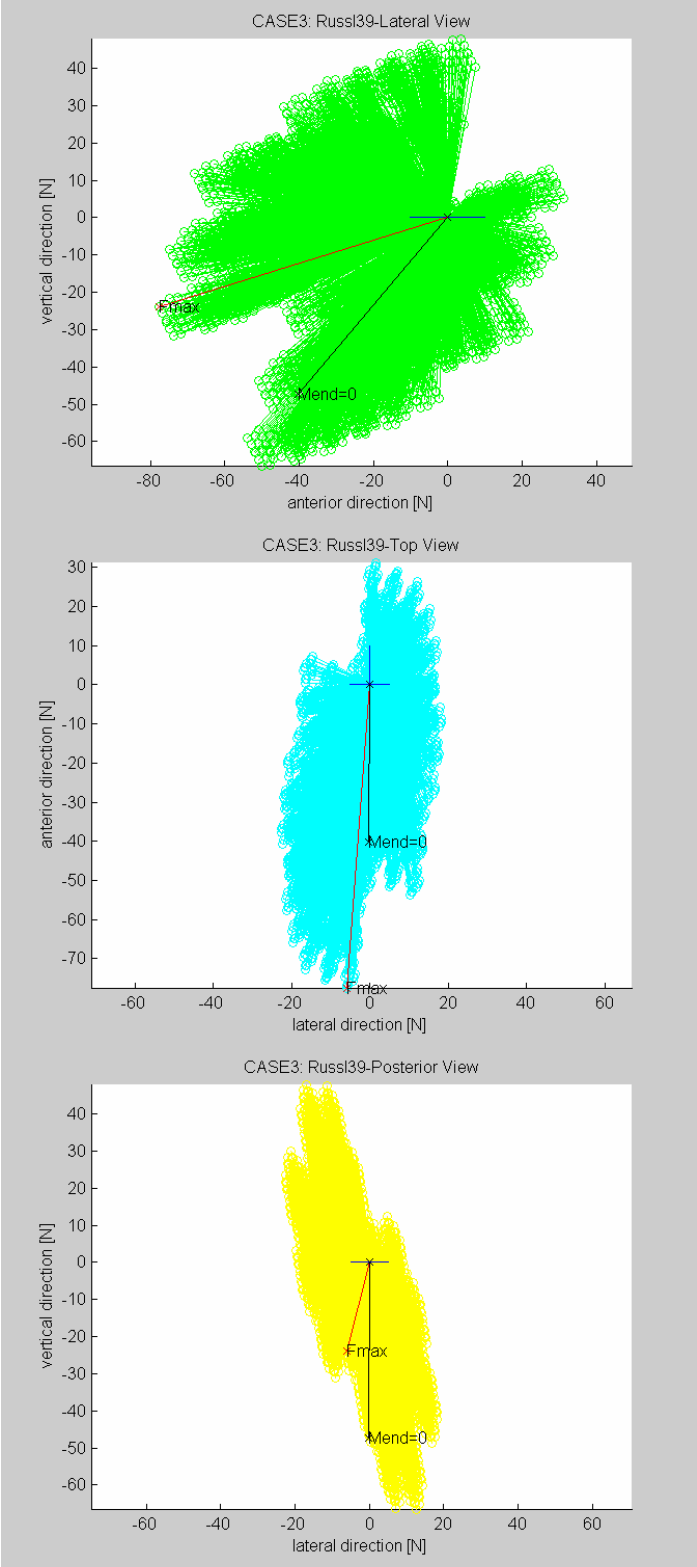

Figure 40: Feasible force set constructed for retracted posture, and unconstrained and constrained optimization results.

4.3.4 Discussion

Muscle coordination patterns accompanying maximum force generation involve submaximal muscle activations to have a stable limb posture. Studies in the literature support constrained end point moment hypothese (Valero-Cuevas, 1998). This finding contradicts results of (Schmidt et al., 2003) in which nine muscles of the human lower limb in the sagittal plane were used to optimize the joint torques while building the feasible set out of bang-bang solutions. The human lower limb study claims that the maximal force the leg produces should be a bang-bang solution without examining sub-maximal activations of muscles.

Our results indicate findings regarding the direction and magnitude of maximum end point forces. As the number of muscles recruited increased, both the constrained and unconstrained maximum end point force increased. The constrained maximum end point force also increased as the stance distance increased. Also, as the stance distance increased, both the constrained and unconstrained maximum end point forces were directed towards the posterior and gravity directions.

A limitation of the force maximization process was ignoring antagonist actions of muscles to maintain static equilibrium. Antagonist muscles cause reciprocal actions around the same anatomical joint they cross. Some antagonist muscles work together to maintain static equilibrium of the hindlimb. There may be submaximal activations of these muscles to keep the leg in static equilibrium. In the force maximization process the procedure ignored this aspect to maximize force output.

Biomechanical constraints affect postural control strategies. The end point force directions, which are in posterior and gravity directions were similar to the forces used in the postural control. The forces generated by the muscles are linearly related to their stimulation levels. To apply higher amount of forces, a muscle is stimulated more. Muscle patterns are chosen such that high range of forces can be produced. For example, while falling, we do not know how much force we need to generate. In postural control, muscles are activated less than their capacity. Muscles, which can apply high forces, are recruited even though the leg will not use it. The neural control mechanism adjusts itself by increasing the muscle fibers recruited.

V. CONCLUSION AND FUTURE WORK

We constructed a cat hindlimb model to predict force production and muscle coordination for balance control. From the three dimensional model with 31 muscles, we extracted moment arms of the muscles. Similarity of the flexion-extension moment arms with the Burkholder model provided confidence in the SIMM model. The Burkholder model moment arms were validated (Burkholder and Nichols, in press). In the comparison between the SIMM model and Burkholder model, some adduction-abduction moment arms were different, but they did not change our results.

A static analysis was used to calculate forces generated at the toe from muscle activations. The Jacobian matrix was used to transform the torques at the joints to the end point forces at the toe. Our static model includes assumptions such as: the joints were not stiff, the pelvis was fixed, and the gravity was not taken into account. Using the static method, isometric force of each muscle was transformed to the toe. Some of these single muscle forces were different than other modeling and experimental results. The difference was due to the assumption of joints being free to move. If joints were constrained, then each muscle could apply an end point force in the direction consistent with the literature values. This motivated our study of the forces generated by multiple muscle activations.

In multiple muscle activations, joint torques were applied across all of the joints. Therefore, the results of multiple muscle activations were more realistic. Sub-maximal

muscle activation patterns were required to produce maximum end point forces. Bang-bang solutions in the feasible force set were unrealistic because the toe could not realistically support the calculated end point moment considering the magnitude of the endpoint force and the length of the foot\.

The maximum end point force corresponding to multiple muscle activations was in the posterior and gravity directions and matched with postural data. Leg extensor muscles apply forces in the same directions. Therefore, extensors were responsible for the maximum end point forces. These biomechanical force capabilities help us to understand the force strategy used by the central nervous system. Although muscle activations are small in postural control, the muscle pattern generating force in the maximum force direction may be recruited. This may be insurance for responding to unexpectedly large perturbations.

5.1 Utilities

This study will provide a technical foundation for movement science. A realistic model of the cat hindlimb was not available because of the limited experimental results that are under specific conditions, the variability and uncertainty of parameters, different kinematic representations, and many methods to solve the redundancy problem. The model will be useful for researchers dealing with cat hindlimb biomechanics or spinal circuitry for motion (e.g. Dr. Nichols, Dr. Macpherson, and Dr. David Bashor from the University of North Carolina at Charlotte).

For a more comprehensive study, our model can be integrated with a motor neuron model. Neuroscience labs are experimenting and modeling motor neuron interactions (Dr. Robert Lee and Dr. Steve Deweerth). The spinal circuitry forms a crucial part in the big picture. The more thorough neural activation signals we have, the closer our model will be to reality. That is, the better the muscle stimulation structures we use, instead of assigning numbers for muscle activation levels, the better the end point force results will be. The directions of maximum end point forces indicate a tendency towards using extensors in the posterior direction for balance control. However, there is not an obvious biomechanical constraint for obstructing the leg to apply forces in other directions. A neuron-muscle interaction can be the cause for using the "force constraint strategy."

Our study is also a framework for defining functional muscle groupings dependent on the end point forces or response strategy (Torres-Oviedo et al., 2003). Our mechanically isolated model can be integrated with the functional muscle groupings, i.e. muscle synergies. It took hours to construct the feasible force set and solve the optimization algorithm on the computer when the muscles were treated as independent entities. Does the Central Nervous System run and solve these algorithms for every position of limbs, joints, muscles, and for every instant of time? More analysis needs to be done to understand the role of various kinematic and kinetic parameters to decrease uncertainty.

Our model is helpful for visualizing and changing the biomechanical level parameters the CNS deals with. Muscles, joint angles, and distances can easily be visualized; joint axes, relative segment positions, and orientations can be altered to do sensitivity analysis;

more d.o.f.s can be added to the musculoskeletal model; segments can further be articulated; muscles and muscle connection points can be added or modified; muscle lengths can be measured. For better estimation of the muscle moment arms, wrapping objects (pulleys in various shapes) can be employed, however, wrapping objects increase the simulation time significantly. Different muscle models other than Hill model can be employed by SIMM. Also, external forces such as gravity can be included in the algorithm of SIMM.

One other utility of our model is it is applicable for various experiments involving different postures of the hindlimb. By changing some parameters in the model, we can understand force capabilities for different postures in three-dimensions. Moment arms can be extracted easily for any positioning of muscles. Joint axes and joint centers can be calculated in a global coordinate system for any posture within feasible limits. These parameters can be plugged into the mechanical analysis to compute a single or a combination of muscles' end point force amounts, directions, and capabilities.

5.2 Limitations

Limitations of our model are mainly due to assumptions made on cat anatomy, joints, and muscles.

Anatomical simplifications in our model may not exactly represent some capabilities of subjects. The more the position of the cat differs from the default posture, the less accurate results will be. The pelvis was fixed, but in reality it is exposed to movement in

perturbations even though the trunk is fixed. Although the toe is articulated anatomically, in our model, it was assumed to be a point. This results to a point contact at the ground and zero moment for static equilibrium.

The joints in our model have fewer degrees of freedom than they have in reality. The relative motion between two bones is constrained by the ligaments, cartilage and other tissues. Totally, there can be six degrees of freedom including translational and rotational motions at an anatomical joint. In our case, this number is decreased to two for each anatomical joint (hip, knee, and ankle).

In the muscle level force calculation process, muscles were greatly simplified by keeping their cross sectional area constant, and other physiological muscle properties uniform as done in many modeling studies in the literature. Considering a muscle as a single big sarcomere is open to question (Winters, 2000). In the joint level force calculation process, muscles were modeled as lines instead of volumes and the connections assumed to be points instead of areas. In reality, muscles like biceps anterior and posterior, and gluteus medius have an area of connection to the hindlimb. This assumption does not change the torque direction of the joint the muscle spans as long as the point of contact is measured reasonably.

In our model, muscle activation patterns were interpolated between the maximally activated and inactivated states. In fact, muscles are not stimulated uniformly and there is

not a single motor drive to each one of them. This issue was addressed in the Future Directions Section below.

5.3 Future Directions

Muscle lengths, most of the moment arms and single muscle force directions of our static model were consistent with the literature values. The discrepancies needs to be further investigated.

More postures could be used to understand the moment arm and single muscle end point force differences between the SIMM model and other results. The moment arms could be compared for incremental changes of joint angles. The abductor-adductor moment arms could be altered to see the effects on the end point forces. Different postures could be utilized to examine the change of single muscle end point forces.

A sensitivity analysis could be done on the constrained maximum end point forces. For example, the maximum force directions corresponding to the hip angle changes could be helpful. Analysis on small end point moment changes could be performed. The constraint could be modified to see the effect of small end point moments on the end point forces. Different computation and optimization methods could be employed. More muscles could be included in the analysis.

Long-term future directions could be composed of building dynamic simulations with feedback control, and modifying this work for clinical applications.

Dynamic simulation and optimization of the hindlimb could be performed by assigning mass and inertia properties to the bones in SIMM. If the simulation is performed in a pelvis and toe fixed condition, extra effort will be needed to maintain a closed loop system. Feedback control could also be employed in the dynamic model. In optimization, the objective function inherent to the algorithm becomes important. An inadequate objective function containing only maximum force production, minimum distance traveled leads to incorrect results. A more comprehensive goal encompassing the minimization of the metabolic rate and stresses at certain muscles should be utilized.

A tool for employing neuron signals could also be built. Instead of assigning numbers to muscle activations, neuron firing rates could be employed. This may require integration with a motor neuron model. The interaction between neural circuits and muscles could be examined before searching for an answer in higher levels such as the Central Pattern Generator.

It could be showed that the same biomechanical principles, calculation and modeling techniques are applicable to humans. Our model integrated with a neuron model could serve for understanding impaired muscle activation patterns. As the simulations are performed, biomechanics knowledge adds up, and spinal circuitry is correlated to the muscle physiology more realistically, resulting knowledge could be used in clinical applications such as rehabilitation of patients, tendon transfers, and prosthesis design.

The effects of the surgical procedures on the muscles and bones, and the causes and effects of injuries could be explored.

REFERENCES

Bean J.C. and Chaffin D.B. (1988). "Biomechanical Model Calculation of Muscle Contraction Forces: A Double Linear Programming Method." Journal of Biomechanics **21(1)**: 59-66.

Burkholder T.J. and Nichols T.R. (2000). "The Mechanical Action of Proprioceptive Length Feedback in a Model of the Cat Hindlimb." Motor Control **4**: 201-220.

Burkholder T.J. and Nichols T.R. (in press). "A Three Dimensional Model of the Feline Hindlimb." Journal of Morphology.

Chen I-Ming, Yang G., Kang In-Gyu (1999). "Numerical Inverse Kinematics for Modular Reconfigurable Robots." Journal of Robotic Systems **16(4)**: 213-225.

Craig J.J. (1986). "Introduction to Robotics." Reading, MA: Addison Wesley.

Ebert-Uphoff I. and Kozak K. (2002). "Review of the Role of Quasi-Coordinates for the Kinematic and Dynamic Modeling of Parallel Manipulators." Proceedings of the Workshop on Fundamental Issues and Future Research Directions for Parallel Mechanisms and Manipulators, Quebec City, Quebec, Canada.

Free S.A. and Delp S.L. (1996). "Effects of Trochanteric Transfer on the Moment Arms, Lengths, and Force-Generating Capacities of the Hip Abductors." Journal of Orthop. Res. **1(14)**: 245-250.

Gonzalez R.V., Buchanan T.S., Delp S.L. (1997). "How muscle architecture and moment arms affect wrist flexion-extension moments." Journal of Biomechanics **30(7)**: 705-712.

Happee R. (1994). "Inverse Dynamic Optimization Including Muscular Dynamics, A New Simulation Method Applied to Goal Directed Movements." Journal of Biomechanics **27(7)**: 953-960.

He J., Levine W., Loeb G. (1991). "Feedback Gains for Correcting Small Perturbations to Standing Posture." IEEE Transactions on Automatic Control **36(3)**: 322-332.

Hof A.L. (2001). "The force resulting from the action of mono- and biarticular muscles in a limb." Journal of Biomechanics **34**: 1085-1089.

Hollister A., Buford W.L., Myers L.M., Giurintano D.J., Novick A. (1992). "The Axes of Rotation of the Thumb Carpometacarpal Joint." J Orthop Res. **10**: 454-460.

Hollister A.M., Jatana S., Singh A.K., Sullivan W.W., Lupichuk A.G. (1993). "The Axes of Rotation of the Knee." Clin Orthop. **290**: 259-268.

Horak F.B. and Macpherson J.M. (1996). "Postural Orientation and Equilibrium." In: Handbook of Physiology, Section 12. Exercise: Regulation and Integration of Multiple Systems, edited by Rowell L.B. and Shepard J.T. New York: American Physiology Society, p. 255-292.

Lawrence J.H. 3rd, Nichols T.R., English A.W. (1993). "Cat Hindlimb Muscles Exert Substantial Torques Outside the Sagittal Plane." Journal of Neurophysiology **69**: 282-285.

Loeb E.P., Giszter S.F., Saltiel P., Bizzi E., Mussa-Ivaldi F.A. (2000). "Output Units of Motor Behavior: An Experimental and Modeling Study." Journal of Cognitive Neuroscience **12(1)**: 78-97.

Loeb G.E. and Richmond F.J.R. (1994). "Architectural Features of Multiarticular Muscles." Hum Mov Sci **13**: 545-556.

Macpherson J.M. (1988a). "Strategies that Simplify the Control of Quadrupedal Stance. I. Forces at the Ground." Journal of Neurophysiology **60**: 204-231.

Macpherson J.M. (1988b). "Strategies that Simplify the Control of Quadrupedal Stance. II. Electromyographic Activity." Journal of Neurophysiology **60(1)**: 218-230.

Macpherson J.M. (1994). "Changes in Postural Strategy with Inter-Paw Distance." Journal of Neurophysiology **71**: 931-940.

Marder E. and Calabrese R.L., (1996). "Principles of Rhythmic Motor Pattern Generation." Physiological Reviews **76(3)**: 687-717.

Murinas K. (2003). "Transformation of Muscular Actions into Endpoint Forces in the Cat Hindlimb During Stance." (Masters Degree) Georgia Institute of Technology.

Nagurka M.L. and Yen V. (1990). "Fourier-Based Optimal Control of Nonlinear Dynamic Systems." Journal of Dynamic Systems, Measurement, and Control **112**: 17-26.

Pandy, M. G., F. C. Anderson, et al. (1992). "A Parameter Optimization Approach for the Optimal-Control of Large-Scale Musculoskeletal Systems." Journal of Biomechanical Engineering-Transactions of the Asme **114**(4): 450-460.

Pandy M.G. and Zajac F.E. (1991). "Optimal Muscular Coordination Strategies for Jumping." Journal of Biomechanics **24(1)**: 1-10.

Pandy M.G., Zajac F.E., Sim E., Levine W. (1990). "An Optimal Control Model for Maximum-Height Human Jumping." Journal of Biomechanics **23(12)**: 1185-1198.

Paul R.R. (1981). "Robot Manipulators: Mathematics, Programming and Control." MIT Press, Cambridge, MA.

Pollard N.S., Gilbert R.C. (2002). "Tendon Arrangement and Muscle Force Requirements for Humanlike Force Capabilities in a Robotic Finger." Proceedings of the IEEE International Conference on Robotics and Automation, Washington, D.C.

Prilutsky B.I., Herzog W., Allinger T.L. (1997). "Forces of Individual Cat Ankle Extensor Muscles During Locomotion Predicted Using Static Optimization." Journal of Biomechanics **30(10)**: 1025-1033.

Raikova R. and Aladjov H.Ts. (2002). "Hierarchical Genetic Algorithm Versus Static Optimization – Investigation of Elbow Flexion and Extension Movements." Journal of Biomechanics **35**: 1123-1135.

Rossignol S. (1996). "Neural Control of Stereotypic Limb Movements." In: Handbook of Physiology, Section 12. Exercise: Regulation and Integration of Multiple Systems, edited by Rowell L.B. and Shepard J.T. New York: American Physiology Society.

Sacks R.D., and Roy R.R. (1982). "Architecture of the hindlimb muscles of cats: Functional significance." Journal of Morphology **173**: 185-195.

Sciavicco L., Siciliano B. (2000). "Modeling and Control of Robot Manipulators." Reading, Great Britain: McGraw Hill Inc.

Schmidt M.W., Lopez-Ortiz C., Barrett P.S., Rogers L.M., Gruben K.G. (2003). "Foot force direction in an isometric pushing task: prediction by kinematic and musculoskeletal models." Exp Brain Res **150**: 245-254.

Schutte L.M., Hayden S.W., Gage J.R. (1997). "Length of Hamstrings and Psoas During Crouch Gait: Effects of Femoral Anteversion." Journal of Orthopaedic Research **15(4)**: 615-621.

Spagele T., Kistner A., Gollhofer A. (1999). "Modeling, simulation, and optimization of a human vertical jump." Journal of Biomechanics **32**: 521-530.

Spector, S.A., Gardiner P.F., Zernicke R.F., Roy R.R., Edgerton V.R. (1980). "Muscle Architecture and Force-Velocity Characteristics of Cat Soleus and Medial Gastrocnemius – Implications for Motor Control." Journal of Neurophysiology **44(5)**: 951-960.

Tarchanidis K.N., Mackay A.S., Lucas J. (1995). "Flexible kinematics for modular robots." Microprocessor and Microsystems **19(9)**: 525-532.

Todorov, E. and Jordan M.I. (2002). "Optimal feedback control as a theory of motor coordination." Nature Neuroscience **5(11)**: 1226-1235.

Torres-Oviedo, G., Macpherson, J.M., Ting, L.H. (2003). "Functional muscle groups controlling ground reaction forces during balance." Society for Neuroscience, New Orleans, LA.

Valero-Cuevas J.F., Zajac F.E., Burgar C.G. (1998). "Large index-fingertip forces are produced by subject-independent patterns of muscle excitation." Journal of Biomechanics **31**: 693-703.

Valero-Cuevas J.F., Johanson M.E., Towles J.D. (2003). "Towards a realistic biomechanical model of the thumb: the choice of kinematic description may be more critical than the solution method or the variability/uncertainty of musculoskeletal parameters." Journal of Biomechanics **36**: 1019-1030.

Winters J.M. (2000). "Biomechanics and Neural Control of Posture and Movement." Reading, WI: Springer-Verlag.

Yamaguchi G.T. (2001). "Dynamic modeling of musculoskeletal motion." Reading, MA, kluwer Academeic Publishers.

Young R.P., Scott S.H., Loeb G.E. (1992). "An intrinsic mechanism to stabilize posture – joint-angle-dependent moment arms of the feline ankle muscles." Neuroscience Letters **145**: 137-140.

Young R.P., Scott S.H., Loeb G.E. (1993). "The distal hindlimb musculature of the cat: multiaxis moment arms at the ankle joint." Exp Brain Res **96**: 141-151.

Zajac F.E., Zomlefer M.R., Levine W.S. (1981). "Hindlimb Muscular Activity, Kinetics, and Kinematics of Cats Jumping to their Maximum Achievable Heights." J. exp. Biol. **91**: 73-86.

Zajac F.E. (1989). "Muscle and Tendon – Properties, Models, Scaling, and Application to Biomechanics and Motor Control." Crit Rev Biomed Eng **17(4)**: 359-411.

Zajac F.E. (2002). "Understanding muscle coordination of the human leg with dynamical simulations." Journal of Biomechanics **35**: 1011-1018.

Zatsiorsky V.M. (2002). "Kinetics of human Motion." Reading, IL: Human Kinetics.